# Joint Centre for Mesoscale Meteorology, Reading, UK

## Mesoscale Effects of a Dry Intrusion within a Vigorous Cyclone

K. A. Browning
B. W. Golding

Internal Report No. 29

May 1994

**Met Office** Joint Centre for Mesoscale Meteorology Department of Meteorology
University of Reading PO Box 243 Reading RG6 6BB United Kingdom
Tel: +44 (0)118 931 8425 Fax: +44 (0)118 931 8791
www.metoffice.com

# Mesoscale effects of a dry intrusion within a vigorous cyclone

K A Browning
Joint Centre for Mesoscale Meteorology*
University of Reading

and

B W Golding
Meteorological Office
Bracknell

* The Joint Centre for Mesoscale Meteorology is supported by the Meteorological Office and the Department of Meteorology, University of Reading.

## Summary

The paper describes the results of a diagnostic study using radar and satellite imagery, together with surface reports and output from regional and mesoscale models, on an occasion of a rapidly deepening cyclone crossing the British Isles. The study shows how air descended from tropopause level in the form of mesoscale dry intrusions which overran parts of the warm conveyor belt ahead of a surface cold front. One of the dry intrusions has been analysed in detail because it led to large changes in the character of the wide frontal rain band: in some places the precipitation became convective, with a tornadic squall line developing, whilst in other places the precipitation was entirely suppressed. Although the effect of the dry intrusion was seen most clearly in the precipitation distribution as determined by radar, the approach of the dry intrusion was also clearly detected in the satellite water vapour imagery and foreshadowed in the model forecasts.

The mesoscale model reproduced many of the observed mesoscale features. It also provided insight into the detailed behaviour of the dry intrusion that led to the tornadic squall line. It showed that the dry intrusion was characterised by a mesoscale filament of high potential vorticity that was extruded from a large region of high PV just above a low tropopause. The extruded PV anomaly that generated the severe weather plunged to within a kilometre of the surface where it overran part of the warm conveyor belt. The warm conveyor belt was itself characterised by a strip of high PV generated locally, mainly by condensation. At the time of the severe weather the model showed the two PV features merging, with part of the low-level PV anomaly rotating cyclonically around the leading edge of the other. The quality of the mesoscale model simulation gives grounds for optimism that such models are capable in principle of predicting severe mesoscale weather events when as

in this case they are orchestrated by resolved larger-scale dynamics. The primary limitations appear to be in the initial data and the convective parametrization used in the model.

## 1. Introduction

There is much interest currently in the dynamics of rapidly deepening mid-latitude cyclones: see, for example, several review papers in the Palmén Memorial Volume (Newton and Holopainen, 1990). An objective is to be able to predict the central pressure of such cyclones, their rate of deepening and the associated pressure gradients. This is important because such cyclones are sometimes responsible for storm force winds (eg the damaging storm of October 1987 in southern England and northern France (Shutts 1990). There are, however, other important aspects that also need to be better understood. The processes that accompany cyclogenesis also lead to characteristic mesoscale distributions of precipitation and convective phenomena. These are difficult to observe because much of the life cycle of such storms generally occurs over the sea where there are few detailed precipitation observations (a notable exception is the study of Wakimoto et al 1992). In the study reported in the present paper a cyclone deepened rapidly as it crossed the British Isles and provided an opportunity to investigate the detailed structure and evolution of the precipitation and accompanying phenomena.

The intense low that provided the opportunity for this study crossed the British Isles on 12 November 1991 (McCallum and Clark 1992; and Lilley 1992). Its frontal system brought heavy rain and thunderstorms in addition to severe gales. Strong squalls accompanied the passage of the cold front and there were two confirmed tornadoes in East Anglia. A damage survey (Pike 1992) indicated that one of the tornadoes was intense.

Winds in the tornado were inferred to have been up to about 70 m $s^{-1}$ when it produced a swath of damage 1 km long in Dullingham, Cambridgeshire, at about 1930 UT. The other tornado, which affected Kirton in east Suffolk about an hour later, was moderate to strong, with inferred windspeeds of up to about 50 m $s^{-1}$. The rate of deepening of the parent low, some hundreds of kilometres to the north, just met the criterion, 24 mb in 24h, for explosive cyclogenesis (Sanders and Gyakum 1980).

Routinely available imagery from the UK weather radar network and from the satellite Meteosat have been analyzed together with output from the regional (50 km grid) version of the operational Meteorological Office Unified Model (Cullen 1991) and the non-hydrostatic mesoscale model (15 km grid) of Golding (1992) to reveal the synoptic and mesoscale structure of this cyclone. Particular importance has been attached to the diagnosis of the intrusion of dry air from the upper troposphere and lower stratosphere into the region of frontal precipitation as in the case studied by Young et al (1987). This 'Dry Intrusion' was clearly revealed by the Meteosat water vapour imagery and by the Unified Model; it was also evident in the radar imagery from the effect it had on the frontal precipitation. As we shall demonstrate, the dry intrusion suppressed the precipitation in many places but, where precipitation did occur, it was convective and intense. The tornadoes were associated with this convection, the tops of which were up to only 5 km or less. Although the analyses and short range forecasts, even from the Mesoscale Model, were not able to reproduce all the details of the incursion of the dry intrusion into the precipitation zone, they nevertheless showed a high degree of consistency with important aspects of the radar and satellite imagery.

## 2. Synoptic setting

Fig 1 shows surface analyses from the Central Forecasting Office for 12 and 18 UT on 18 November 1991. They differ in detail from the analyses presented later but nevertheless show the broad picture. The already intense secondary low pressure centre over southern Ireland at 12 UT deepened a further 16 mb by the time it reached SE Scotland at 18 UT. The mesoscale weather events that are discussed in this paper occurred in association with the frontal system to the south of this secondary cyclone as it crossed Britain.

Fig 2 shows an infra-red image from Meteosat depicting the cloud system at 18 UT. The main features are (i) a frontal cloud band associated with a major warm conveyor belt (WCB) extending from west of Biscay towards Scandinavia, and (ii) a well defined dry slot, with a hooked cloud head to the north of it, on the western side of the frontal cloud band over SE Scotland. The cloud head formed in association with the intense low that travelled from Ireland to Scotland. Another cloud head can be seen farther north, associated with another low pressure centre between Scotland and Iceland.

The major WCB showed up well in the regional model's humidity field (see light grey strip in Fig 3). The relative flow was strong along its axis, especially from Brittany to the North Sea and on to the north of Scotland. The correspondence between the model-derived 'cloud' pattern (Fig 3) and imagery (Fig 2) is quite close, even down to the individual cloud heads over and to the north of Scotland. Figures 3 and 2 both show the dry intrusion curving northwards over England and Wales, terminating in SE Scotland at the centre of the low. The more detailed analyses given later show that the overall dry intrusion seen here was composed of two features: one of them (referred to as Dry Intrusion 1) tracked NE'wards from southern Ireland to Scotland, while the other (Dry Intrusion 2) tracked eastwards from southern Ireland across southern Britain and was associated with the tornadoes.

The present case resembled other recently analyzed examples of rapid cyclogenesis (eg Young et al 1987, Whitaker et al 1988, Shutts 1990, Reed et al 1992) in that it was characterised by coupling between frontogenesis in the upper and lower troposphere. In terms of the potential vorticity paradigm (Hoskins et al 1989), the rapid cyclogenesis occurred when a region of high potential vorticity (PV) in the lower stratosphere and upper troposphere (Fig 4(c)) encroached upon a diabatically-generated strip of high PV associated with air of high wet-bulb potential temperature ($\Theta_w$) at low levels within the WCB (Fig 4(a)). The dry intrusion that is the focus of attention in this paper (later called Dry Intrusion 2) was associated with a downward extension of the region of locally very high PV over west Wales in Fig 4(c).

The upper-level PV=2 region (stratospheric air) extended down almost to 600 mb. Individual maxima, corresponding to downward extensions of the peak values in Fig 4(c), were located farther to the south at the lower levels than at 300 mb. They gave rise to the individual cores within the PV strip which can be seen in Fig 4(b) curving from west of Biscay northwards over England and Wales. The low-level PV strip in Fig 4(a) extended upwards to give the broad strip in Fig 4(b) that is situated over the eastern side of England and over the North Sea. The PV features of upper-level and lower-level origin came closest together over southern England. At the resolution of the regional model, a downward penetrating local PV maximum at 600 mb can just be seen located over eastern Devonshire, within about 200 km of the maximum PV at 900 mb. We return in Section 4 to a more detailed examination of the PV structure as derived from the mesoscale model. In the meantime we shall concentrate on the observational analysis of the dry intrusion and its effects.

## 3. Mesoscale observational analysis of the dry intrusion and its effect on the precipitation

### (a) Dry intrusion as seen in water vapour imagery

Observational evidence of the dry intrusion is provided by the Meteosat water vapour imagery (Fig 5). A dark zone, indicative of very low humidity in the upper and middle troposphere, can be seen sweeping across Britain behind the deep band of moist and mainly cloudy air associated with the WCB. Fig 5 shows that the dark zone appeared initially as a single entity, but as it approached England and Wales at 15 UT it elongated and split into two dark zones. One of these, labelled Dry Intrusion 1, travelled NE'wards towards Scotland, coincident with the low pressure centre. The other, labelled Dry Intrusion 2, travelled eastwards across the southern half of England and Wales.

### (b) Effects of the dry intrusion as seen by radar

On the weather radar network display the effect of the overall dry intrusion could be seen at 13 UT (Fig 6(a)) as the large dry slot between Ireland and SW England. The rain to the north of it, over Ireland, was associated with the developing cloud head immediately to the northwest of the low pressure centre. The belt of continuous rain to the east, extending from SW England up the west coast of Wales, was associated with the WCB. The transition from continuous rain to patchy showery rain (cellular radar echoes) marks the eastern edge of the dry intrusion. The rear edge of the dry intrusion was situated some way behind the showery rain whose western boundary was itself just ahead of the boundary of the high-$\theta_w$ surface flow associated with the WCB.

The showers beneath the dry intrusion intensified at 14 UT along a roughly north-south line extending from north Wales to the English Channel (Fig 6(b)). The sequence of hourly plots in Fig 7 depicts the rapid eastward progression of heavy showers within this line. A significant feature of Fig 7 is the dearth of heavy showers over southwest England. This was the region beneath that part of the overall dry intrusion referred to as Dry Intrusion 2 as it swept across southern Britain. After 17 UT, however, there was an abrupt change beneath this part of the dry intrusion: where previously the convection had been suppressed, it suddenly developed as an intense squall line with local rainfall intensities of order 100 mm $h^{-1}$. This squall line travelled, beneath the core of Dry Intrusion 2, into East Anglia where between 1930 and 2030 UT the two tornadoes occurred. At this time there was a major step or dislocation between the squall line and other parts of the line further south over France.

(c) Detailed analysis at 18 UT

Fig 8 shows the radar network display at 18 UT during the development of the intense squall line. The band of continuous rain associated with the WCB can be seen extending from NW France across the eastern part of East Anglia; parts of it can also be seen near the maximum radar range to the north of the Wash. (The intensity of the rain within the band of continuous rain over SE England is exaggerated by a radar fault but this does not influence the present discussion). Behind the continuous rain in eastern England is the region affected by the dry intrusion where, apart from the squall line, the rain is suppressed. Near the southern boundary of the dry intrusion, over NW France, one of the narrow rainbands within the band of continuous rain corresponds to line convection.

An analysis of surface pressure and dewpoint from the many stations reporting at 18 UT is given in Fig 9. It shows that the squall line over central southern England was associated with a sharp surface trough. So, too, was the line convection over NW France. Both these features were close to the axis of maximum surface dewpoint. A rather gradual decrease in dewpoint occurred behind them. The sharpness of the pressure troughs is attributed to moist processes (latent heat sources and sinks) accompanying the lines of heavy rain. Over the Channel at this time there was a gap between the squall line and the line convection characterized by only weak showers, and so the trough there is shown as a relatively smooth feature.

Figure 10 is a synthesis (a - plan view; b - vertical section) of the 18 UT observations from surface stations, radar and infra-red and water vapour imagery. Fig 10(c) is a simplified interpretation of Dry Intrusion 2, where the dashed line denotes the horizontal extent of the dry intrusion, the arrows depict relative flow within the dry intrusion and the stippled band represents the WCB flow. The western boundary of the WCB aloft is taken to be defined by the sharp drop in the cloud tops (scalloped line in Fig 10(a)). At the surface, the western boundary of the WCB flow can be taken to be approximately where the dewpoint dropped below about 6°C (solid line in Fig 10(a)). Behind these boundaries, which lay roughly one above the other, the dry slot was seen as the dark zone in the water vapour imagery. Ahead of these boundaries, the dry intrusion, although obscured by overlying WCB cloud, was manifested in the radar display by the suppression of continuous rain from the WCB.

The intense squall line, with tops to only 5 km or less, developed within the region of suppressed WCB rain, where the dry intrusion overran the region of highest surface

dewpoints as shown in Fig 10(b). This overrunning resembles a kata-cold front and the model of Browning and Monk (1982). Occurrences of dry intrusions overrunning air with high-$\theta_w$ ahead of the surface fronts have been reported in other studies of explosively deepening cyclones (eg Young et al 1987, Wakimoto et al 1992, Kuo et al 1992). The main difference in this case is that the dry intrusion overran only the lower portion of the WCB, not the entire depth of the WCB flow; in other words it appeared to penetrate into the WCB, undercutting part of it.

Evidence of some undercutting by the dry intrusion is provided by multiple-elevation azimuth scans by the operational Chenies (London) radar which showed the rear edge of the widespread rain to be rather farther west at 4 km than at 2 to 3 km. Presumably precipitation generated within the region of slantwise ascent was evaporating where it fell into the dry intrusion.

The reason for the convection becoming intense within the newly developing squall line is intriguing because it reflects a nice balance between two opposing effects of the dry intrusion: Although the dry intrusion, as shown in Sec 4, was characterized by a low $\theta_w$, it would have arrived in this region with a relatively high temperature, having had a previous history of dry descent (except where precipitation from aloft evaporated within it). Indeed the region with the maximum potential instability was initially the region with the least opportunity to realize it because it was where the descent had been strongest. However, the air was by then re-ascending so that eventually the potential instability was realized. Representing the balance between these effects so as to reproduce the correct timing of the onset of convection is a major challenge for numerical weather prediction (NWP).

The pattern of flow in the region of line convection over NW France was different from that just described in relation to the squall line over England. Fig 11 shows that the French line convection developed from a row of convective showers that encroached upon the band of uniform WCB rain from the west (see arrow). As the showers penetrated they evolved from moderately intense individual cells (Fig 11(a)) to a more intense narrow cold frontal rainband (Fig 11(c)) corresponding to archetypal line convection (Browning 1990). Although the position of the leading edge of the dry intrusion is shown in Fig 10(a) to have been 50 to 100 km behind the line convection, it must be remembered that this was its position as defined by the rear edge of continuous rain. In this region the continuous rain is thought to have been associated with rearward sloping ana-cold frontal ascent above a wedge of dry intrusion air that would have extended to the position of the line convection close to the surface and was probably responsible for sustaining it.

## 4. Analysis of the dry intrusion using NWP model products

### (a) Vertical velocity field as represented in the regional model

We have already shown, in Fig 3, the regional model representation of the broad pattern of relative humidity characterizing the WCB and the dry intrusion behind it. Fig 12 shows the associated patterns of vertical velocity in the low and middle troposphere. The feature that stands out is the long band of ascending air associated with the WCB. The band was wider at 500 mb than at 900 mb and, at its western edge aloft, ascent extended above regions of descent associated with the dry intrusion. In particular, Fig 12(a) shows two core regions of descent ahead of the broad region of descent: One of these, east of Scotland, was associated with Dry Intrusion 1. The other, with a small (but, as we shall see, highly

significant) maximum centred over the south coast of England, was associated with Dry Intrusion 2. A cross-section through Dry Intrusion 2 shows the dry descending air, with low $\theta_w$, intruding into the moist high-$\theta_w$ air of the WCB. Details of this important intrusion process are clarified using the mesoscale model (see Sec 4b).

The region of descent behind the WCB, depicted in Fig 12, led to a large area of relatively dry air at the surface as shown in Fig 13. The overall dry area is an amalgam of three distinct pools of dry air labelled 1, 2 and 3. The model-derived flow in the 12°C isentropic surface has been calculated in a frame of reference moving with the overall system (270°, 20 m $s^{-1}$) and the principal features of the resulting flow pattern are represented in Fig 13 by the three pairs of arrows near the labels 1, 2 and 3. These correspond to the diffluent flows associated with Dry Intrusions 1 and 2 over the British Isles and to a much larger dry intrusion over mid-Atlantic.

(b) The dry intrusions as represented by the mesoscale model

The Unified Model assimilation was rerun at mesoscale resolution (about 16.7 km grid spacing) for the period 06 -12 UT to generate initial conditions for the mesoscale model simulation. A feature of this assimilation was the treatment of the 12 UT sounding from Valentia in southwest Ireland. This observation implied strong horizontal shear on the northern flank of the jet at middle and upper tropospheric levels. In the regional model assimilation, quality-control checks rejected this sounding because it differed too much from the first guess. However, it was accepted at most levels in the mesoscale-resolution assimilation, presumably because of a better resolution of the shear by the finer grid. For consistency, the initialisation for the simulations presented below was generated from a re

-assimilation in which these quality-control checks were overridden, so that all levels of the sounding were used.

The results of this re-assimilation were used, after interpolation, to initialise a 15-km gridlength, 16-level simulation using the non-hydrostatic mesoscale model described in Golding (1992,1993). The model uses a split semi-implicit formulation and semi-Lagrangian advection. Turbulent mixing is parametrized using variables conserved during condensation and a prognostic turbulent kinetic energy (TKE) equation. The cloud scheme is coupled to the TKE equation by fractional cloudiness, and uses a bulk formulation of liquid and ice cloud microphysics. Convection is parametrized using an instability-related closure and uses resolved dynamics to redistribute the transported mass.

An overview of the model simulation is provided by Fig. 14 which shows surface pressure, wind and precipitation. The location of the overall squall line, from Cherbourg in north France to northeast England, is close to that observed (Figs. 8 and 9) and shows the dislocation over the English Channel. The most intense part of the squall line, over central southern England, is depicted as a region of heavy convective rain with maximum grid-mean rain rates in excess of 10mm $hr^{-1}$. Mean 10m winds exceed 30km close to the squall with a 90° veer over two gridlengths, and surface gusts of 65kn are indicated by the magnitude of the 300m wind. The region of stratiform rain ahead of it is also well depicted. There is a gap between the heaviest stratiform rain and the main squall line but, for reasons that will be discussed, the magnitude of the gap is underestimated and it does not extend far enough to the northeast in the model (Fig. 10 shows that it should extend to the Wash). The narrow rainband extending into SW England from the northern end of the main squall in central England, can be associated with an observed band of showers which, however, did not have the continuity or intensity of the model simulation.

Figure 15 shows a 3-hourly sequence of relative humidity at 1.5km above msl from the mesoscale simulation. The development of Dry Intrusion 2 is clearly shown in the forward edge of the post-frontal air as it travels from southern Ireland towards SE England. The shape of this intrusion was particularly sensitive to assimilation of the Valentia ascent. The main part of the dry intrusion at this level is shown to have relative humidities substantially less than 80%, and even below 40% in places. However, Fig. 15(c) shows that, just to the east of the main intrusion at 18 UT, there is a further eastward extension of fairly dry air (RH between 80 and 100%) in the region where Fig. 14 shows the model to have been producing convective outbreaks. As we shall demonstrate shortly in connection with Fig. 21(c), this is where air with low $\Theta_w$ or equivalent potential temperatures ($\Theta^e$) associated with the dry intrusion was overrunning air with higher $\Theta_e$ associated with the WCB. The observed position of the squall line at 18 UT, just to the north of the Isle of Wight (Fig. 8), corresponds well with the narrow finger of saturated air in Fig. 15(c) located within this region of overrunning. This process of overrunning continued so that by 21 UT the only sign of the squall line in the model's humidity pattern is the finger of air with RH greater than 60% over the Straits of Dover (Fig. 15(d)). We suspect that in reality this pattern of overrunning should have been present also at earlier stages in the model integration.

The vertical structure of the dry intrusion at 18 UT is illustrated in Fig. 16 by the superposition of the 60% relative humidity contours at 1.5km and 4km. It shows the dry air associated with Dry Intrusion 2 advancing farthest ahead at the lower level. At even lower levels, in the boundary layer, the humidity remained high. Key features of the sequence in Fig. 15 are replotted in Fig. 17 to focus attention on the way in which the driest part of the dry intrusion thrust forward and eventually became cut off at the lower level. This is the region where the observations showed that the precipitation was generally suppressed except,

notably, for the very intense squall line. The squall line developed after 18 UT ahead of the northern end of the region of driest air shown in Fig. 17, and by 21 UT it was associated, as previously noted, with the moist finger protruding into the northern end of the same region of dry air which by then had overrun to a greater extent.

The structures of the potential vorticity (PV) maxima associated with the two dry intrusions are illustrated in Fig. 18 which shows the evolution of the PV=1 contour on the 25°C and 19°C isentropic surfaces. These surfaces correspond roughly to the centres of the respective PV anomalies. Note the formation of a hammer-head shape for each intrusion as it developed, due to diffluent flow at its leading edge. The 25°C analysis in Fig.18(a) shows mainly Dry Intrusion 1 (see shaded areas) although the upper part of Dry Intrusion 2 can also be detected in this surface. The 19°C analysis in Fig. 18(b) shows Dry Intrusion 2 alone. A complication discussed shortly is that there were two distinct regions of origin for air with high PV: one was within the dry air coming down from high levels and the other was within the moist low-level air in the WCB. On the 19°C surface (Fig. 18(b)) it became impossible at 21 UT to separate the upper anomaly from the lower one, generated by diabatic processes, so the combined anomaly is shown at 21 UT.

Evidence of Dry Intrusion 2 having descended from upper levels is given in Fig. 19 which shows time sequences of (a) PV=1 and (b) 60% relative humidity contours, on the 19°C isentropic surface, together with the height contour associated with their leading edges. The descent was particularly rapid between 12 and 15 UT: this is more than 1km in 3 hours, corresponding to an average descent rate of 10 cm $s^{-1}$. Further confirmation was obtained by advecting a tracer whose initial value was the 12-UT PV field, modified to be zero below

3.5km and wherever the relative humidity exceeded 90%. The results (not shown) confirmed that upper-level air of high PV was advected down to below 2km.

We have already drawn attention to the fact that, although the features depicted in Figs. 18 and 19 were mostly of high-level origin, there were other areas of high PV situated ahead of the dry intrusion which were of low-level origin and generated by local diabatic processes. The relationship between these two areas of high PV is shown for 18 UT in Fig. 20; here a lower (16°C) isentropic surface has been chosen to highlight the lower part of Dry Intrusion 2. The 60% relative humidity contour in Fig. 20 emphasises the close relationship of the dry intrusion and the high-PV air of high-level origin over southwest England. In contrast, the high-PV air of low-level origin was associated with moister (generally cloudy) air in the WCB. The diagram emphasises the close proximity at this time of the dry, upper-level PV anomaly and the saturated, lower-level PV anomaly over central southern England. The small finger of high-PV air of low-level origin over Wales originated ahead of the front in the WCB. In a relative frame of reference, it had been carried cyclonically around the advancing tongue of high-PV air of high-level origin and then left behind at about 2.5km as a moist, high-PV area resembling a miniature version of a "bent-back occlusion" or "bent-back warm front".

The vertical structure of Dry Intrusion 2 is shown in Fig. 21 for 15 and 18 UT along the line A-B in Fig. 16. The overall structure in Fig 21 is broadly similar to the observationally deduced structure shown in Fig. 10(b). Note, for example, the rear edge of the high-humidity region, corresponding to ice cloud, sloping upwards from left to right between the middle troposphere and the upper troposphere. Note also the dry low-$\Theta_e$ air undercutting the moist WCB air below 4km and the extension of slightly drier air just ahead of the squall line between 15 and 18 UT, creating a region of strong potential instability, the

parametrized release of which is indicated by the asterisks in Fig. 21. This aspect of the simulation was found to be sensitive to the partitioning between grid scale and sub-grid scale mass flux, an excess of grid scale uplift leading to underestimation of the true dryness (and potential instability) just ahead of the squall line. The observed squall line intensified after 18 UT, leading to the tornadoes in East Anglia between 19 and 21 UT. These were evidently the culmination of processes resulting from the dry intrusion penetrating into the WCB. A detailed study of this interaction is underway, using the model at much finer resolution, and will be reported separately.

We have just shown that, at the same time that the dry intrusion was undercutting a large part of the WCB cloud mass, it was also overrunning moist air from part of the WCB that was being left behind within the boundary layer. This led to the shallow but vigorous upright convection at the squall line, as just described, but in the model it also led to a further squall line more than 100km behind the main squall. This second squall line was associated with the moist high-$\Theta_e$ WCB air that had travelled (relatively) rearwards as part of the previously mentioned "bent-back" frontal feature (note that the surface dewpoint analysis in Fig. 9 confirms the rather delayed drop in $\Theta_e$ depicted by the model). The model's second squall line can be seen in Figs. 21(c) and (d) extending to about 3km beneath the overrunning dry intrusion. The maximum of PV below the intrusion at this location is the result of the diabatic processes in the low-level convection. The observations in this area indicate only isolated convection resulting from release of the instability rather than a second squall line as produced by the model.

## 5. Concluding remarks

We have described the structure of a dry intrusion, its evolution and its effect on the mesoscale distribution of weather, from a purely observational point of view in Sec 3 and by means of NWP model diagnostics in Sec 4. Our study reveals some of the strengths and weaknesses of the observations and models. It also reveals something about the atmospheric processes at work, raises a number of key issues and points up the potential for improved short-range forecasting of severe weather.

### (a) Strengths and weaknesses of the observational data.

For studying and forecasting mesoscale events such as these, the best data routinely available are satellite and radar imagery. Once again the ability of water vapour imagery to detect and track significant dry intrusions has been demonstrated. However, these features develop rapidly and, in this case, no more than 12 hours was available between the first appearance of an insignificantly small dark zone in the satellite imagery and the development of the squall line. Thus the predictive value of the imagery may be limited, but its nowcasting value may be rather greater in terms of diagnosing what is going on and for tracking the location of the centre of activity. Its value can best be exploited by interpreting the satellite imagery together with the radar imagery to account for the occurrence and non-occurrence of rain, its pattern, and the distribution of statiform versus convective rain. The relationship between model products and the imagery is also instructive: a key approach is to validate model-derived forecasts of relative humidity and potential vorticity against the water vapour imagery, taking into account the possibility of a dry intrusion being partially obscured beneath higher-level cloud.

(b) Strengths and weaknesses of the NWP models.

The broad features of humidity and precipitation distribution for this case were captured well by the 50 km - gridlength regional model even though it failed to reproduce the rapid deepening of the low centre. However, many of the severe weather features, in particular the precipitation-related events, were organized on the mesoscale, and it is more appropriate to look to a mesoscale model to represent them. The tornadoes themselves were even smaller-scale phenomena but they are likely to have been the outcome of dynamical organization on the scales resolvable by mesoscale model.

The non-hydrostatic mesoscale model with 15 km gridlength used in this study was successful in reproducing the location, strength and the limited vertical extent, of the main squall line, and also the associated pressure and wind distribution. It provided a clear picture of the enhancement of the squall line in the region of the dry intrusion as the associated high-PV air intruded from aloft into the warm conveyor belt and partially overran some of the warm moist boundary-layer air.

The most obvious weaknesses in the model representation were in developing the French line convection rather too far east of its true position, in developing too much convection behind the main squall line over England, and in underestimating the extent of penetration of dry air ahead of the main squall line. This last deficiency is a critical one and is probably symptomatic of the model's sensitivity to the convective parametrization. We suspect that the present convection scheme was transporting too much mass in the grid scale updraught. What appears to be required in the model is for the convection to be more strongly constrained by the overrunning dry intrusion such that

(1) there would be less convective erosion of the dry intrusion as it penetrates into the WCB, and

(2) the convection, where it does break out, would do so in a more concentrated and violent manner.

Severe convection of this kind requires some form of localized mesoscale forcing to overcome the resistance to convection and this will not be easy to represent.

Another factor limiting the performance of the model is the initial data. The fact that the model underestimated the penetration of the dry intrusion into the WCB as it overran warm moist boundary-layer air may, as in the case of its failure to deepen the cyclone sufficiently, be due to inadequate initialization as well as to faulty parametrization. Further research is needed to assess the relative importance of these limitations. It is expected that a useful way forward will be to experiment with the non-hydrostatic mesoscale model at even higher resolution.

(c) Nature of the atmospheric processes.

Dry intrusions are typical features of cyclone development (Browning and Roberts 1994). But they are not usually associated, as in the present case, with the development of such a vigorous squall line. Even less often in NW Europe are they associated with generation of damaging tornadoes. More case studies will be needed to put this case properly into perspective but what appears to have made it unusual was the strength and nature of the large-scale atmospheric circulation that brought fast-moving, high-PV air rapidly

down from tropopause level into a strong low-level baroclinic zone. Here it overran a boundary layer containing air with high $\Theta_w$ and high PV generated diabatically.

It is not clear whether it is mainly the high PV of this dry intrusion air or its dryness, or both, that bestows such dynamical importance on the dry intrusions. Nor is clear whether the generation of PV and convective instability by melting and evaporation is as important as their generation by condensation. These issues, together with a better understanding of the interaction between the PV anomalies of upper and low-level origin, are matters that can best be addressed by future high-resolution modelling studies.

Finally, although it is the mesoscale aspects of the dry intrusion once it penetrated into the low troposphere that were responsible for the details of the severe weather, it is likely that it was the larger-scale distribution of PV in the vicinity of the tropopause that orchestrated the rapid descent of the dry intrusion in the first place. Such a perspective would help account for the rather high degree of predictability of the mesoscale features studied in this paper.

**Acknowledgements**

We are grateful to M Hackett, G Holpin and R Lilley at the Meteorological Office, Bracknell, for provision of radar and satellite data and to P Ferris and N Roberts for generating radar, satellite and model output.

## References


| | | |
|---|---|---|
| Browning, K.A. | 1990 | 'Organization of clouds and precipitation in extratropical cyclones'. In extratropical cyclones: Erik Palmen Memorial Volume, Amer.Meteorol.Soc., Boston, Mass., pp 129-153. |
| Browning, K.A. and Monk, G.A. | 1982 | 'Simple model for the synoptic analysis of cold fronts'. Q.J.R.Meteorol.Soc., **108**, 435 452. |
| Browning, K.A. and Roberts, N. | 1994 | Structure of a frontal cyclone. Q.J.R.Meteorol.Soc., **120**, In press. |
| Cullen, M.J.P. | 1991 | 'The Unified Forecast/Climate Model', Short Range Forecasting Division Scientific Paper No. 1, Meteorological Office, Bracknell. |
| Golding, B.W., | 1992 | 'An efficient non-hydrostatic forecast model' Meteorol. Atmos. Phys., 50, 89-103. |
| Golding, B.W., | 1993 | 'Numerical prediction of a severe storm in Melbourne' Aust.Met.Mag, 42, 47-57. |
| Hoskins, B.J., McIntyre, M.E. and Robertson, A.W. | 1985 | 'On the use and significance of isentropic potential vorticity maps'. Q.J.R.Meteorol.Soc., **111** 877-946. |
| Kuo, Y-H., Reed, R.J. and Low-Nam, S. | 1992 | 'Thermal structure and airflow in a model simulation of an occluded marine cyclone'. Mon.Wea.Rev., **120**, 2280-2297. |
| Lilley, R.B.E. | 1992 | 'Satellite and radar images - 12 November 1991. Meteorol.Mag., **121**, 26-28. |
| McCallum, E. and Clark, G.V. | 1992 | 'Use of satellite imagery in a marked cyclogenesis on 12 November 1991'. Weather, **47**, 241-246. |
| Newton, C.W. and Holopainen, E.O. | 1990 | Eds., Extratropical cyclones. The Erik Palmen Memorial Volume. Amer.Meteorol.Soc., Boston, Mass. |

| | | |
|---|---|---|
| Pike, W.S. | 1992 | 'The two East Anglian tornadoes of 12 November 1991 and their relationship to a fast-moving triple pint of a frontal system'. Journal of Meteorol., **17**, 37-50. |
| Reed, W.J., Stoelinga M.T. and Kuo, J-H. | 1992 | 'A model-aided study of the origin and evolution of the anomalously high potential vorticity in the inner region of a rapidly-deepening marine cyclone'. Mon.Wea.Rev., **120**, 893-913. |
| Sanders, F. and Gyakum, J.R. | 1980 | 'Synoptic-dynamic climatology of the 'bomb'', Mon.Wea.Rev., **108**, 1589-1606. |
| Shutts, G.J. | 1990 | 'Dynamical aspects of the October storm, 1987: A study of a successful fine-mesh simulation'. Q.J.R.Meteorol.Soc., **116**, 1315-1347. |
| Wakimoto, R.M., Blier, W. and Liu, C. | 1992 | 'The frontal structure of an explosive oceanic cyclone: airborne, radar observations of ERICA IOP-4'. Mon.Wea.Rev., **120**, 1135-1155. |
| Whitaker, J.S., Uccellini, W. and Brill, K.F. | 1988 | 'A model-based diagnostic study of the rapid development phase of the Presidents' Day cyclone'. Mon.Wea.Rev., **116**, 2337-2365. |
| Young, M.V., Monk, G.A. and Browning, K.A. | 1987 | 'Interpretation of satellite imagery of a rapidly deepening cyclone'. Q.J.R.Meteorol.Soc., **113**, 1089-1115. |

## Figure Legends

Fig 1 Surface analyses for (a) 12 UT and (b) 18 UT, 12 November 1991 from CFO Bracknell.

Fig 2 Meteosat infra-red imagery showing the cyclonic cloud system at 18UT, 12 November 1991.

Fig 3 Regional Model 6-h forecast valid at 18 UT, 12 November 1991, showing 500 mb relative humidity (black <60%, grey 60 to 90%, pale grey ≥ 90%) and 500 mb flow relative to the system (white wind vectors plotted relative to a velocity of 20 m $s^{-1}$ from 270°). The area and projection is identical to that in Fig 2. The 500 mb level is a compromise level which is able to portray, in a broad sense, the two principal synoptic scale flows: the long curved tongue of high relative humidity corresponding to the warm conveyor belt, and the major tongue of low relative humidity behind it corresponding to the dry intrusion.

Fig 4 Regional Model 6-h forecast products valid at 18 UT, 12 November 1991, showing

(a) PV at 900 mb (light, medium and heavy shading corresponds to PV = 0.2, 0.6 and 0.8 units) plus $\Theta_w$ at 900 mb (isopleths at 1°C intervals),

(b) PV at 600 mb (increasingly bold shading for 0.2 PV, 0.6 PV and then at intervals of 0.2 PV units to 1.4),

(c) PV at 300 mb (increasingly bold shading at intervals of 1 PV unit, dark shading over Wales corresponding to 8), plus 300 mb isotachs (2.5 $ms^{-1}$ intervals above 50 m $s^{-1}$).

Fig 5 Meteosat water vapour imagery for 12 November 1991:

(a) and (b), respectively, show enlarged views, with stepped grey scale, of the dark zone at 12 UT (before the dry intrusion split) and 21 UT (after the split); the dashed envelopes show the estimated true extent of the dry intrusion allowing for some dry air having extended ahead of (both above and below) the cloudy WCB air.
(c) shows a sequence of tracings of 'level 110' showing the water vapour dark zone at 3-h intervals from 03 to 21 UT.

Fig 6 Weather radar network displays for (a) 13 UT and (b) 14 UT, 12 November 1991. Light, moderate (>1 mm $h^{-1}$) and heavy (>4 mm $h^{-1}$) rain is shown as light, moderate and heavy shading, respectively.

Fig 7 Tracings from the radar network display at hourly intervals from 14 to 21 UT, 12 November 1991, showing the distribution of all rain exceeding 4 mm $h^{-1}$ that occurred in the region of the overall dry intrusion.

Fig 8 Weather radar network display for 18 UT, 12 November 1991. Intensity scale as in Fig 6.

Fig 9 Analysis of surface pressure and dewpoint at 18 UT, 12 November 1991.

Fig 10 Synthesis of dry intrusion at 18 UT, 12 November 1991: (a) plan view, (b) vertical section along $X_1$, $X_2$ in (a), and (c) schematic interpretation (same area as (a)).

Fig 11 Southern portion of weather radar network display for (a) 1430 UT, (b) 1630 UT and (c) 1830 UT, 12 November 1991.

Fig 12 Regional Model 6-h forecast fields of vertical velocity valid at 18 UT, 12 November 1991, (a) at 900 mb and (b) at 500 mb. Contours are at intervals of 2 cm $s^{-1}$. Areas of upward motion are shaded. Note the -2 cm $s^{-1}$ closed contour at low level over the south coast of England situated beneath a broad region of ascent aloft.

Fig 13 Regional Model 6-h forecast field of surface relative humidity valid at 18 UT, 12 November 1991. Areas in excess of 70, 80 and 90% are denoted by light, medium and dark shading, respectively. Drier areas, shown white, are related to three dry intrusions, labelled 1, 2 and 3. The associated arrows represent relative flow as explained in the text.

Fig 14 Mesoscale Model 6-h forecast for 18 UT, 12 November 1991 showing surface pressure (isopleths at 2 mb intervals), wind (each whole barb represents 5 m $s^{-1}$), rainfall intensity (light, medium and heavy stipple corresponds to rain in excess of 0.1, 1.5 and 3 mm $h^{-1}$, respectively) and regions of convective rain (open and solid triangles correspond to local rates in excess of 0.4 and 2 mm $h^{-1}$, respectively).

Fig 15 (a-d) Mesoscale Model analysis for 12 UT (a) and forecasts for 15, 18 and 21 UT, 12 November 1991 (b, c and d), showing relative humidity at 1.5 km above msl. Contours are at intervals of 10%. Saturated regions are shaded.

Fig 16 Boundaries of dry air (RH <60%) obtained from the Mesoscale Model showing the relative positions of Dry Intrusion 2 at 1.5 and 4 km as it crossed southern Britain at 18 UT, 12 November 1991. AB marks the location of the cross sections in Fig 21.

Fig 17 Tracings for 12, 15, 18 and 21 UT, 12 November 1991, showing the evolution of Dry Intrusion 2 as depicted by the Mesoscale Model at the 1.5 km level. Contours are shown for relative humidities of 50 and 60%. The dry intrusion feature is highlighted by shading.

Fig 18 Three-hourly plots of PV=1 within isentropic surfaces obtained from the Mesoscale Model for the period 12 to 21 UT, 12 November 1991. (a) shows the 25°C isentropic surface, within which Dry Intrusion 1

was best defined. (b) shows the 19°C isentropic surface and Dry Intrusion 1. The two dry intrusions are highlighted by shading.

Fig 19 Three-hourly plots for the period 12 to 21 UT, 12 November 1991, showing the evolution within Dry Intrusion 2 of (a) PV≥1 and (b) relative humidity < 60% within the 16°C isentropic surface as depicted by the Mesoscale Model. The dry intrusion feature is highlighted by shading. Also shown (thin lines) are height contours through the lowest parts of these features.

Fig 20 Mesoscale Model 6-h forecast for 18 UT, 12 November 1991 showing PV and relative humidity within the 16°C isentropic surface. Stippled shading shows PV≥1; areas heavily shaded are of upper-level origin and those lightly shaded are of low-level origin. The bold line shows the 60% relative humidity contour. The thin lines give the height of the isentropic surface at 500 m intervals.

Fig 21 Forecast cross-sections from the Mesoscale Model for (a & b) 15 UT and (c & d) 18 UT, 12 November 1991. (a) and (c) show the equivalent potential temperature structure overlaid on the flow in the plane of the section relative to the motion of the simulated squall line (270°C, 25 m $s^{-1}$). (b) and (d) show the relative humidity structure (shading), the cloud boundary (dashed contour) and potential vorticity

(solid contours). Note that relative humidity is with respect to water saturation.

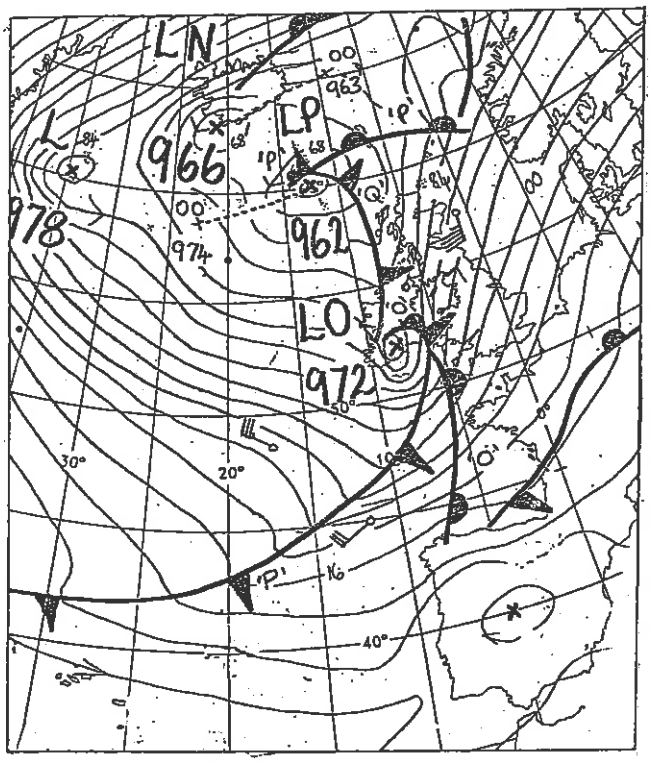
LN
966
LP
963
'P'
978
974
962
LO
972
'Q'
'O'
30°
20°
10°
0°
40°
50°
16

Fig 1 (a)

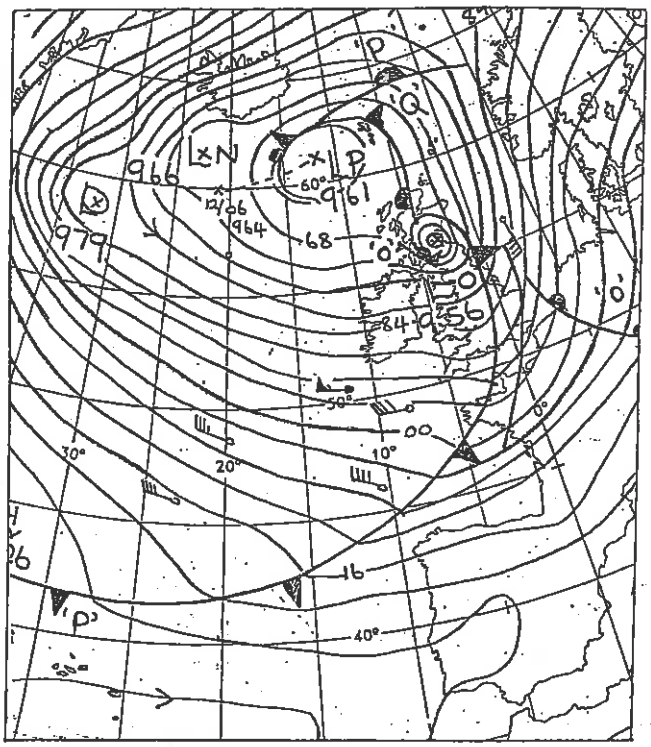
'P'
'Q'
LN
966
961
979
964
68
'O'
956
84
50°
00
30°
20°
10°
16
40°

Fig 1 (b)

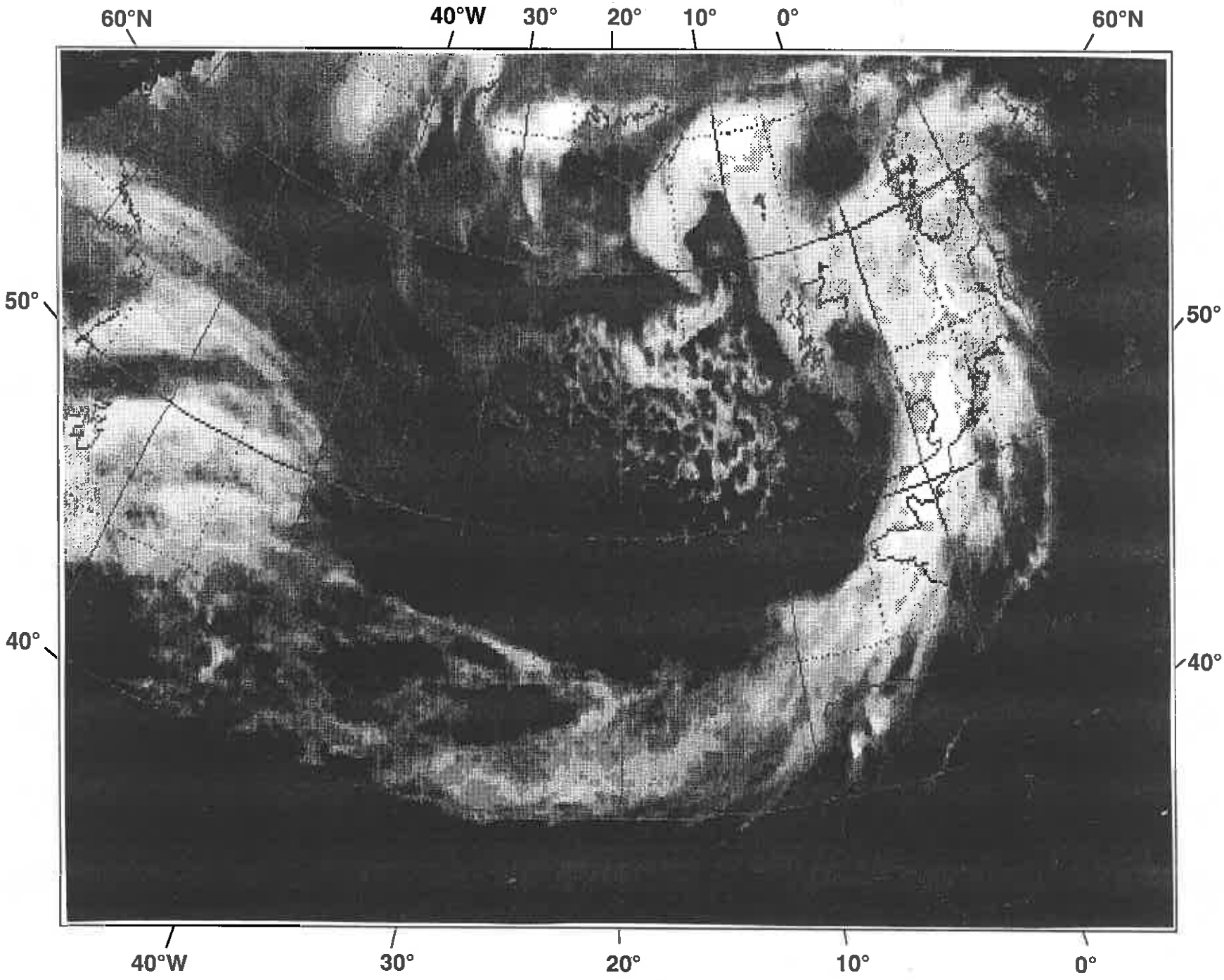


Fig 2

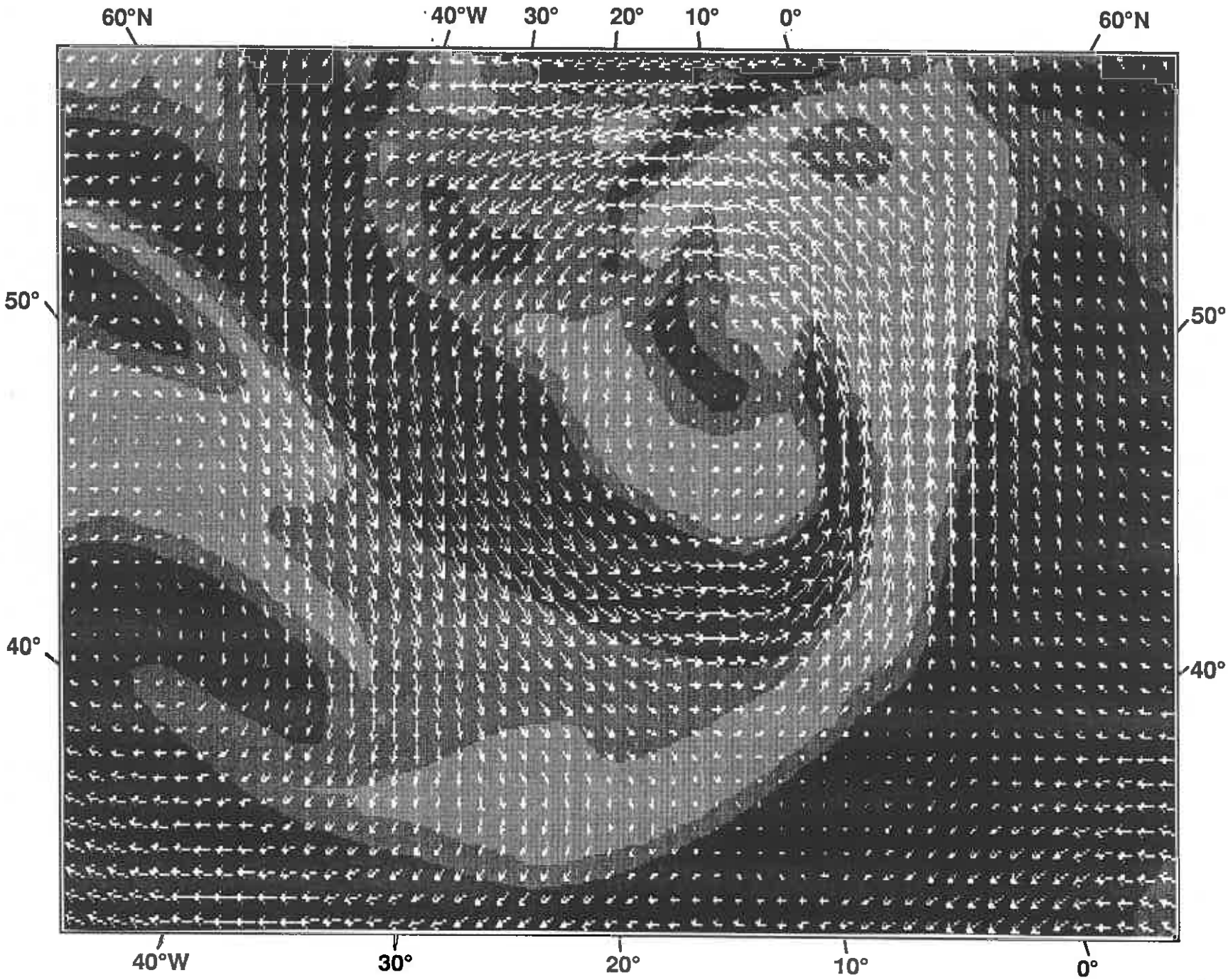


Fig 3

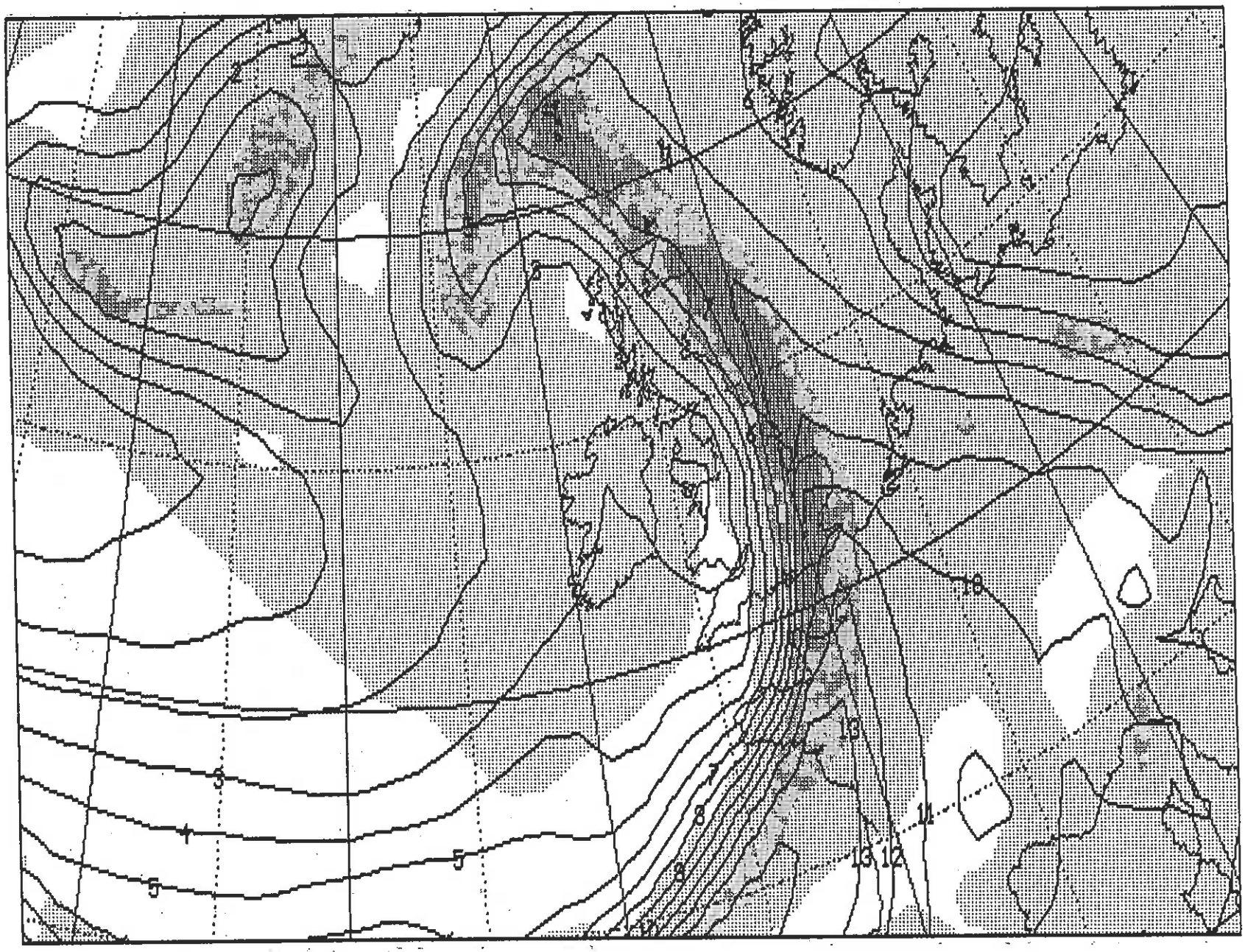


Fig 4(a)

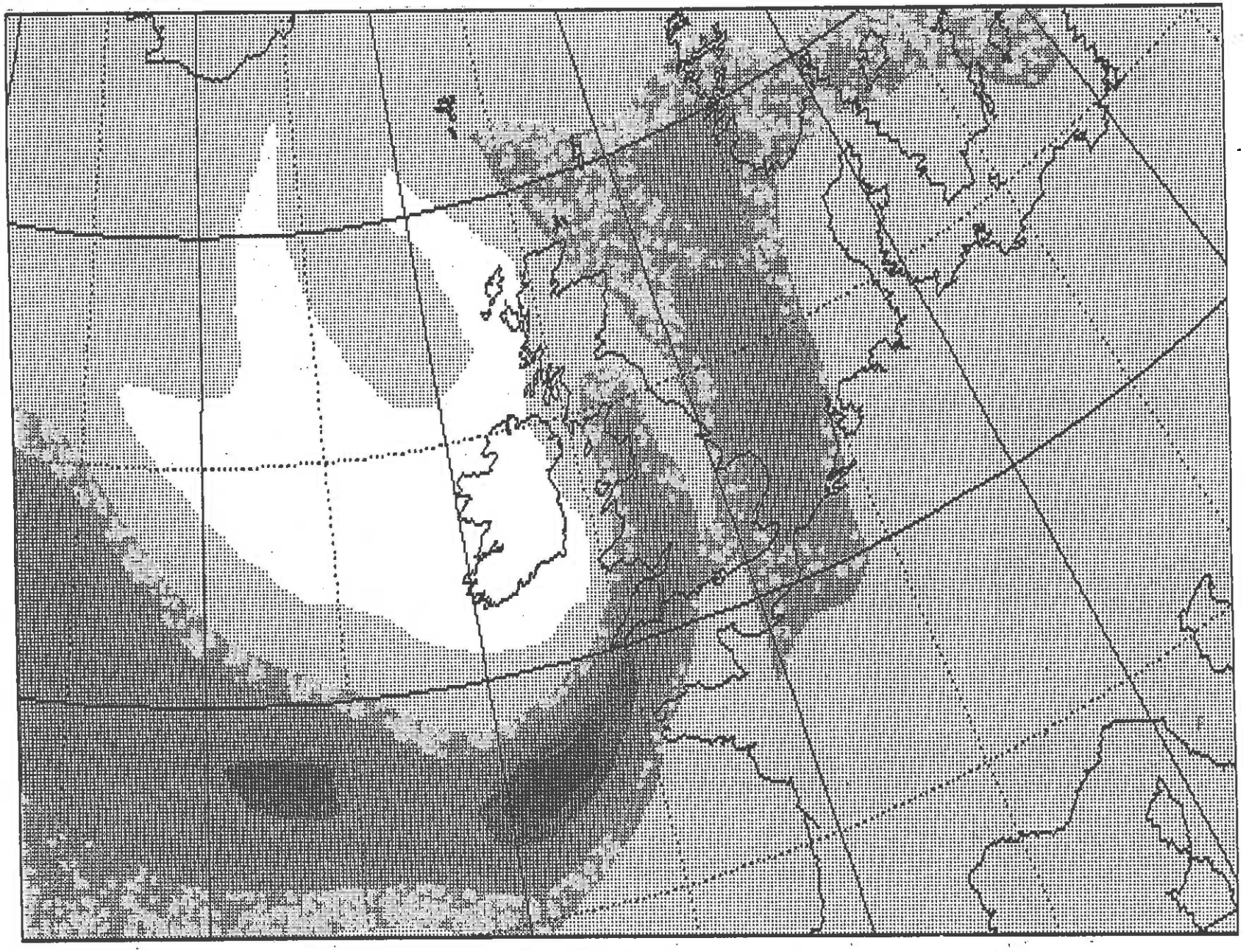

Fig 4 (b)

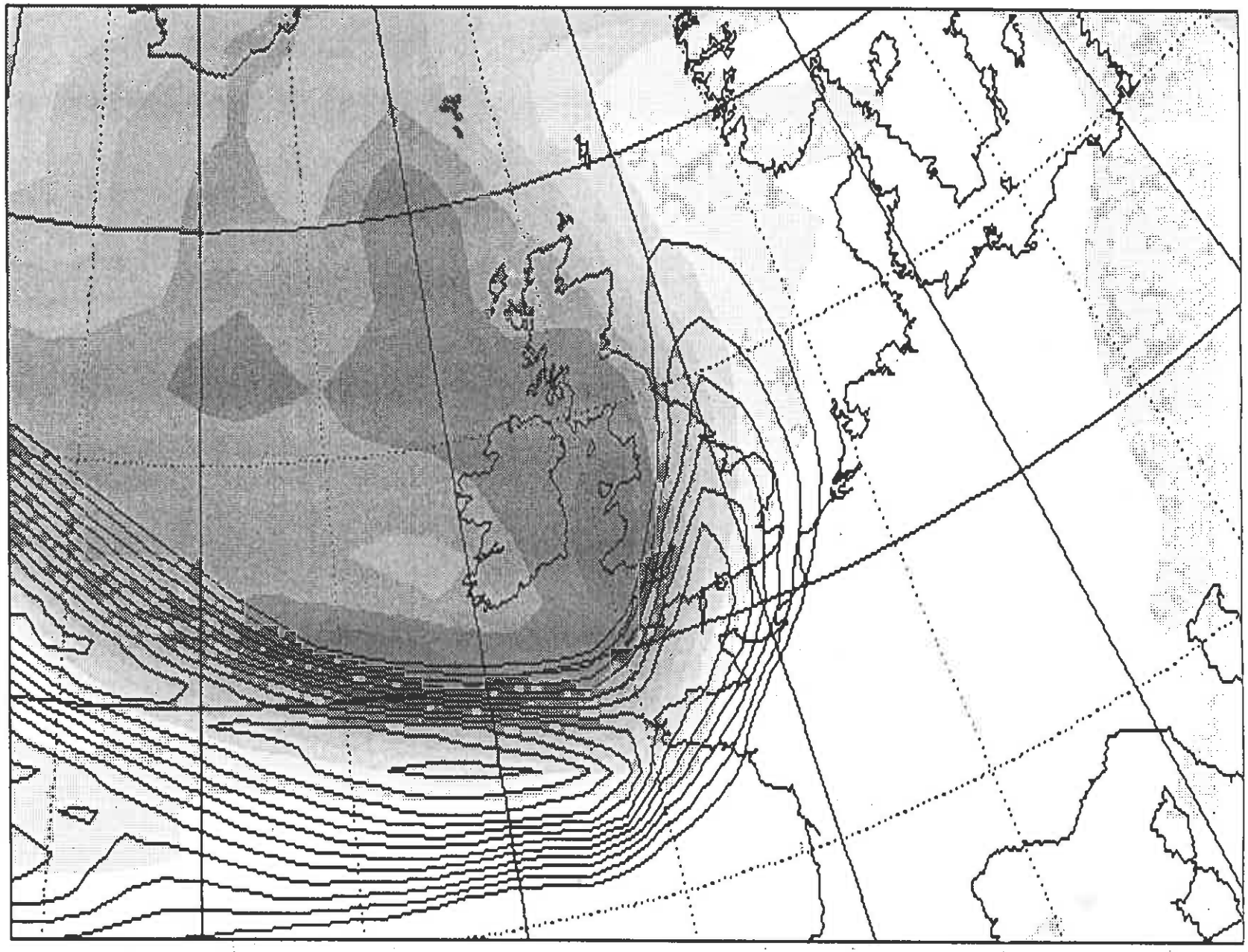

Fig 4(c)

Fig 5(a)

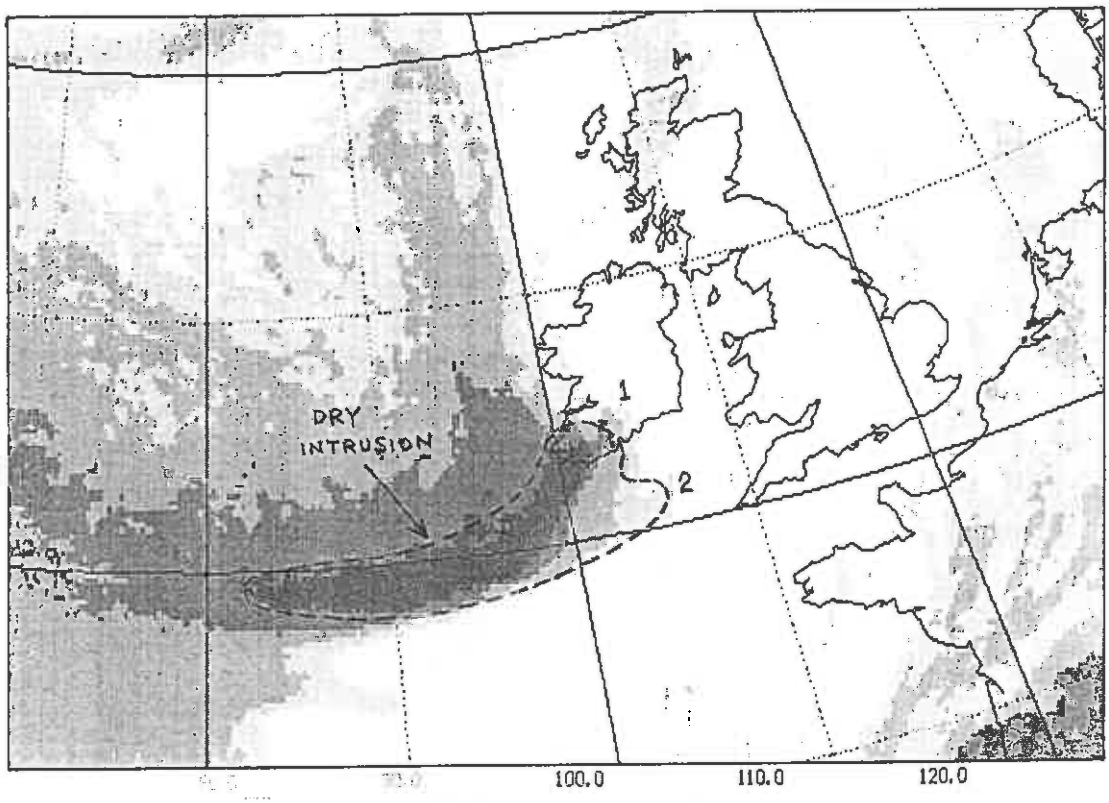


Fig 5(b)

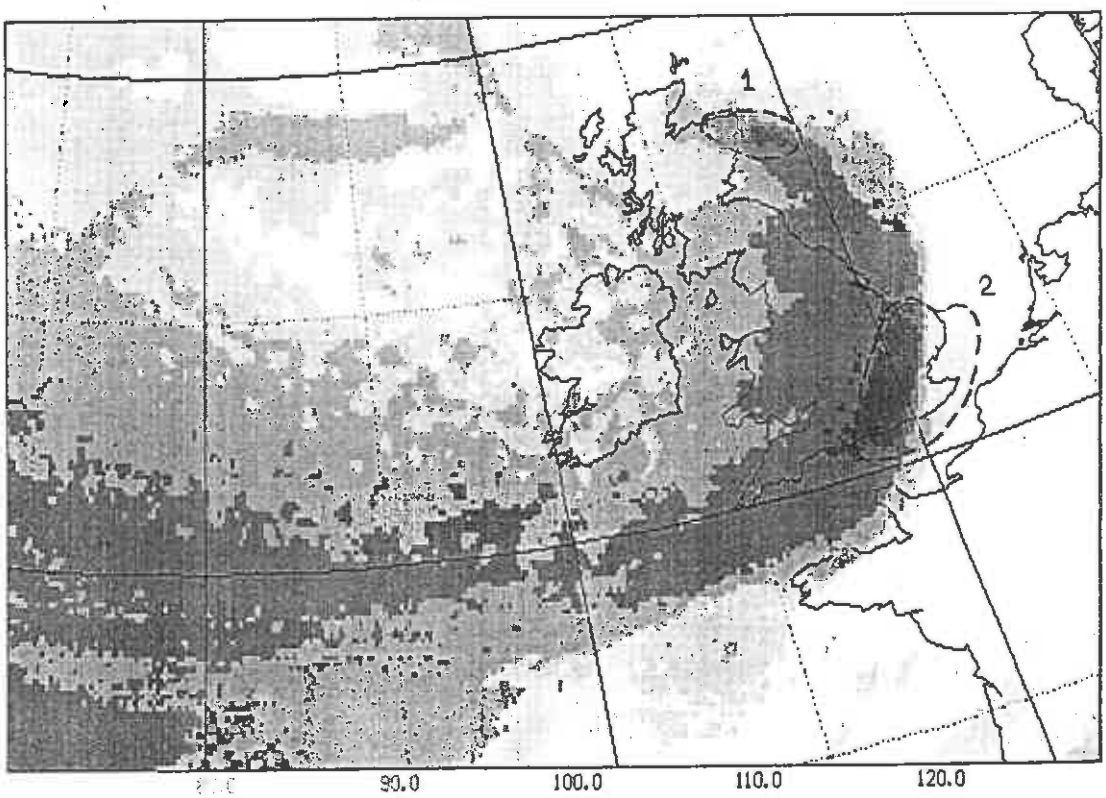

Fig
5(c)

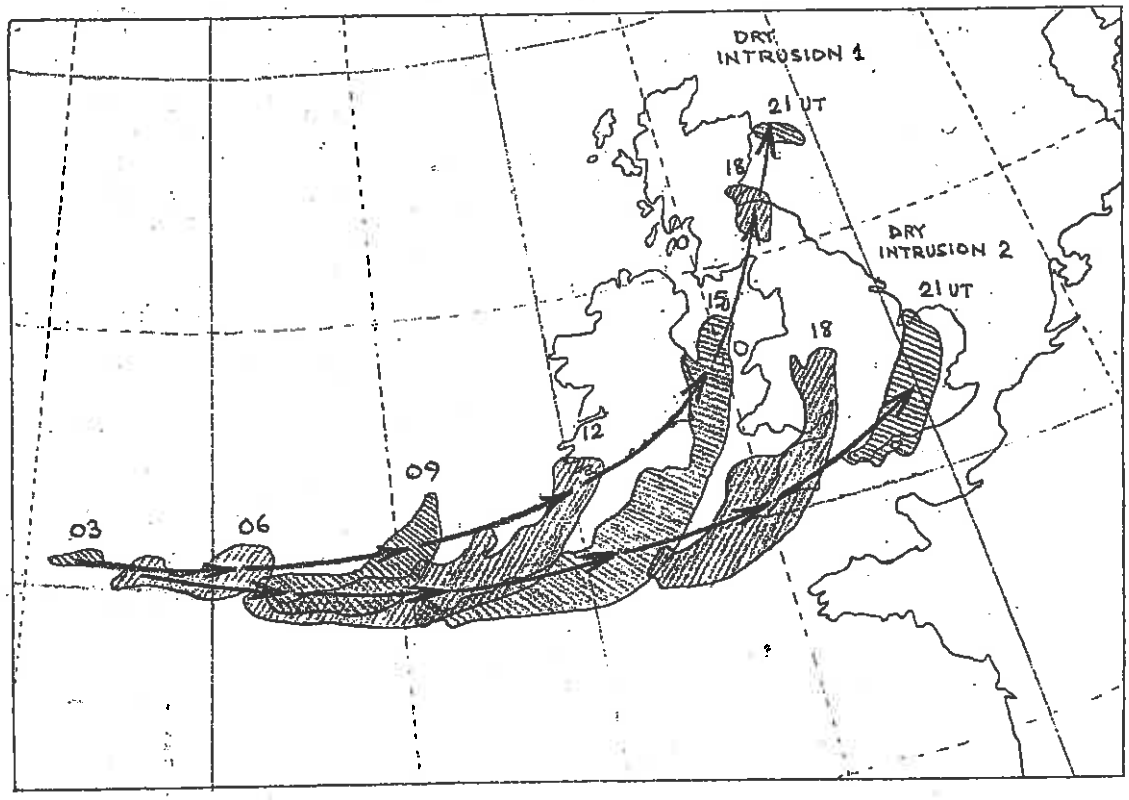

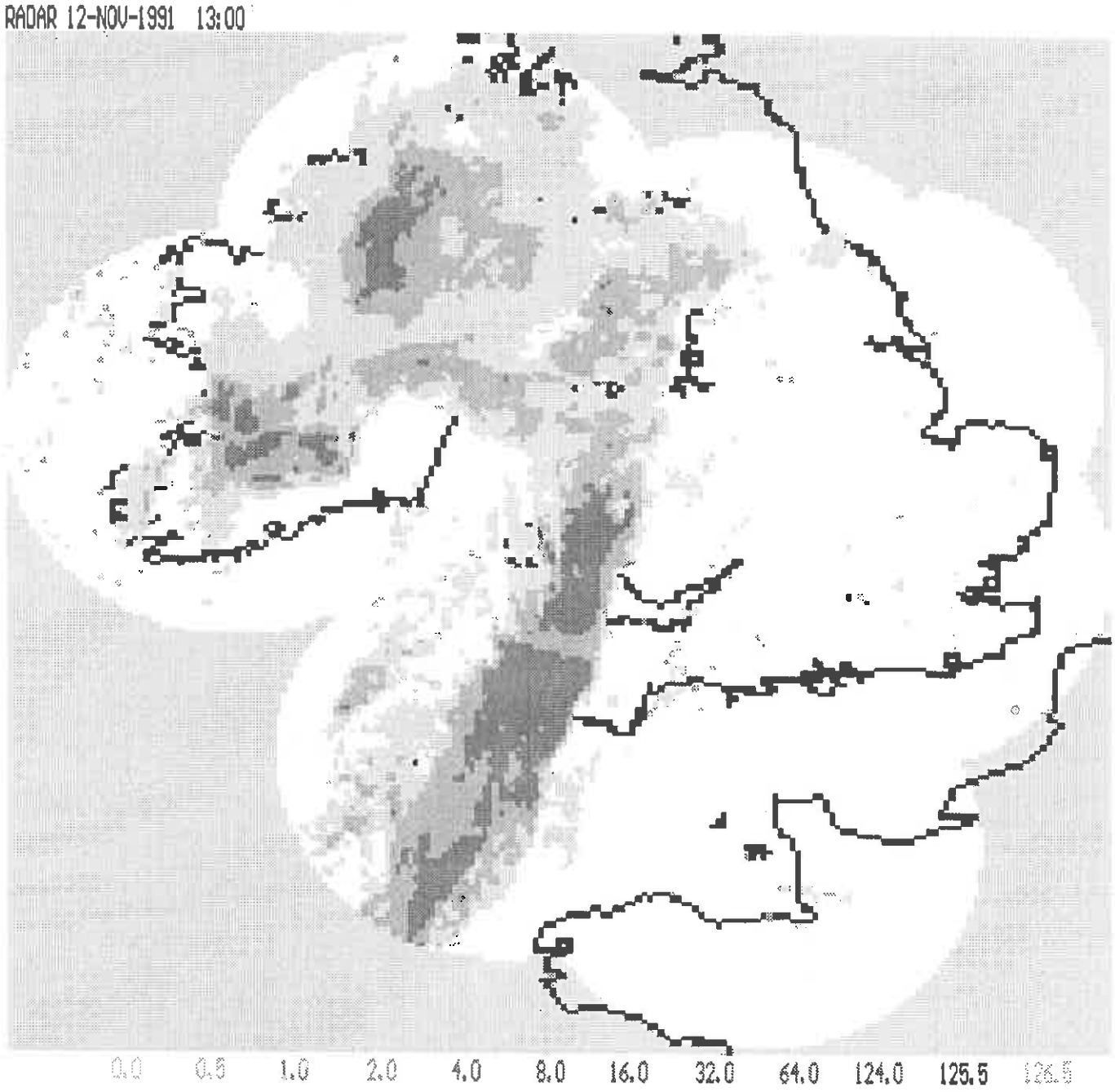
RADAR 12-NOV-1991 13:00
0.0
0.5
1.0
2.0
4.0
8.0
16.0
32.0
64.0
124.0
125.5
126.5

Fig 6(a)

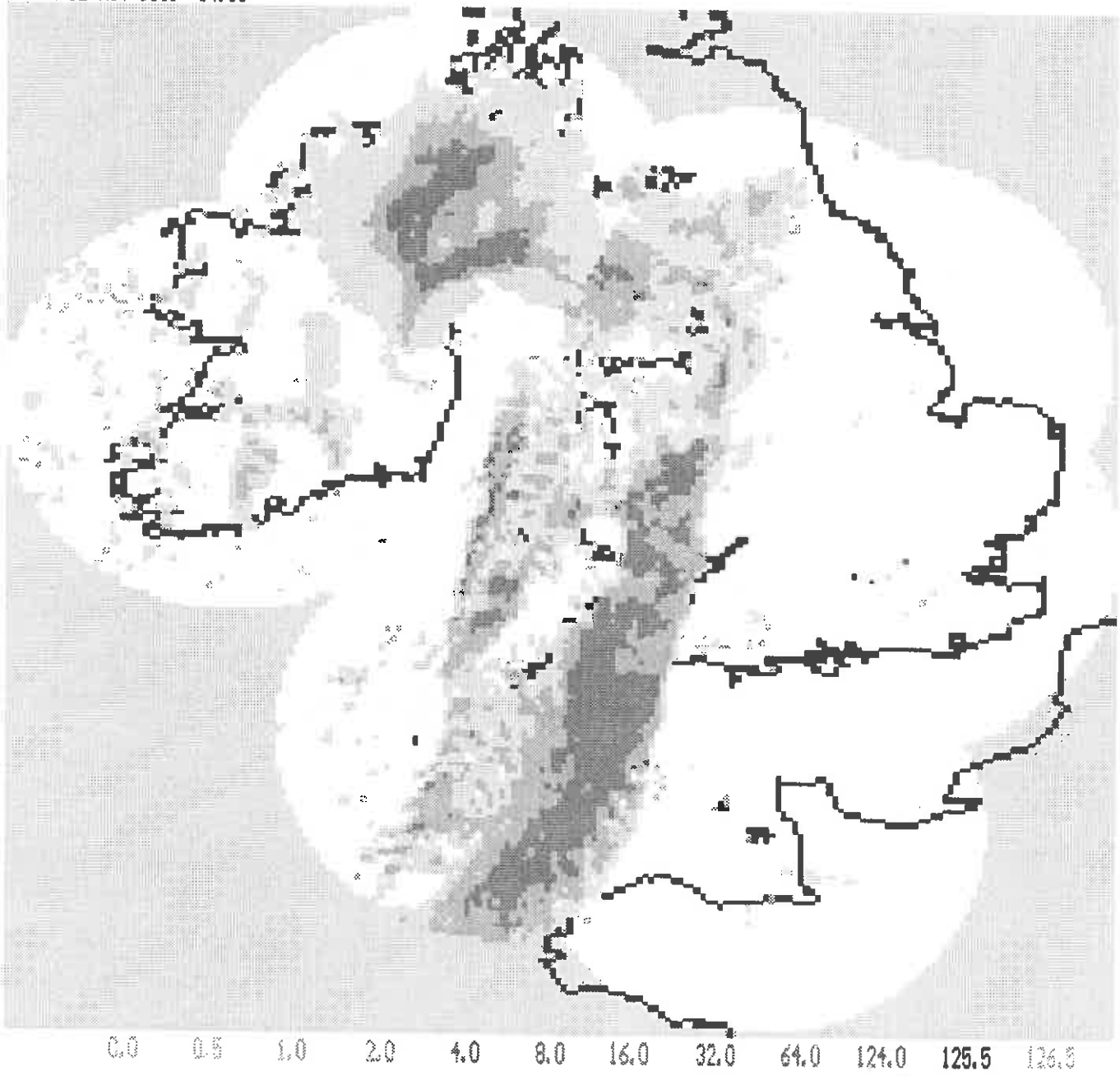
RADAR 12-NOV-1991 14:00
0.0 0.5 1.0 2.0 4.0 8.0 16.0 32.0 64.0 124.0 125.5 126.5

Fig 6(b)


Fig 7

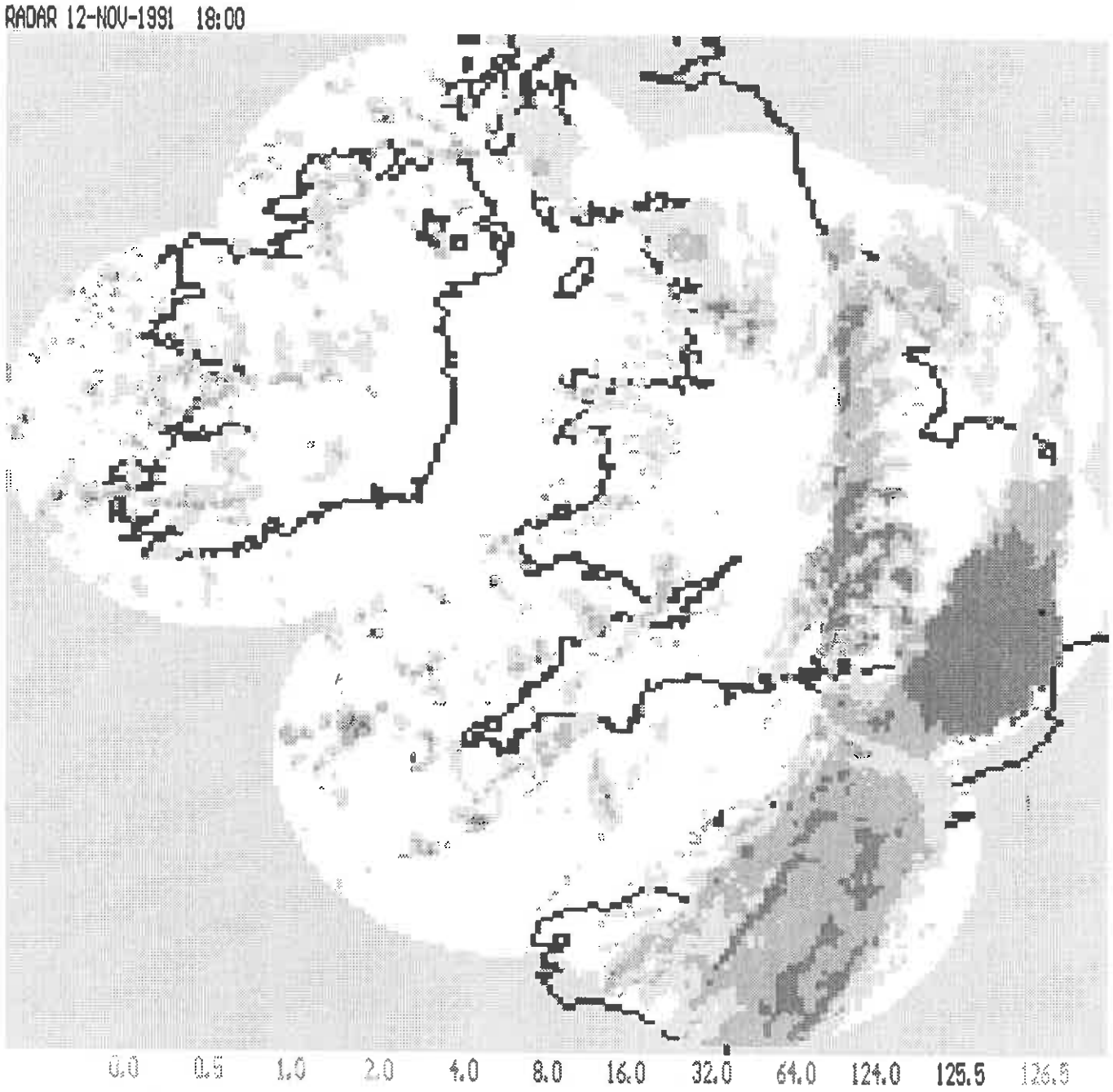
RADAR 12-NOV-1991 18:00
0.0
0.5
1.0
2.0
4.0
8.0
16.0
32.0
64.0
124.0
125.5
126.5

Fig 8

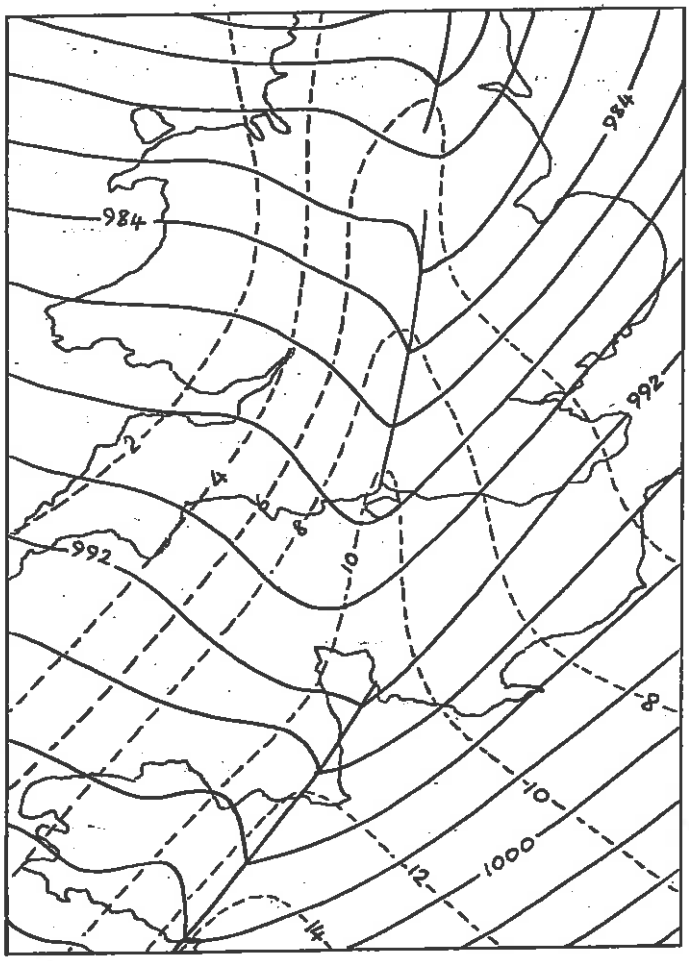


Fig 9

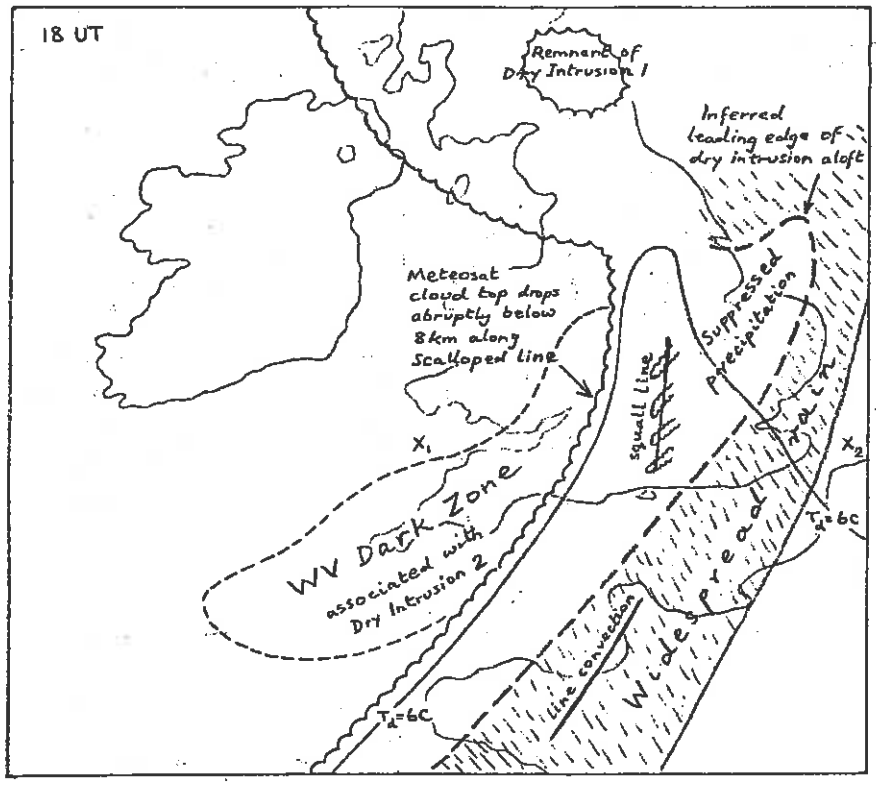


Fig 10(a)

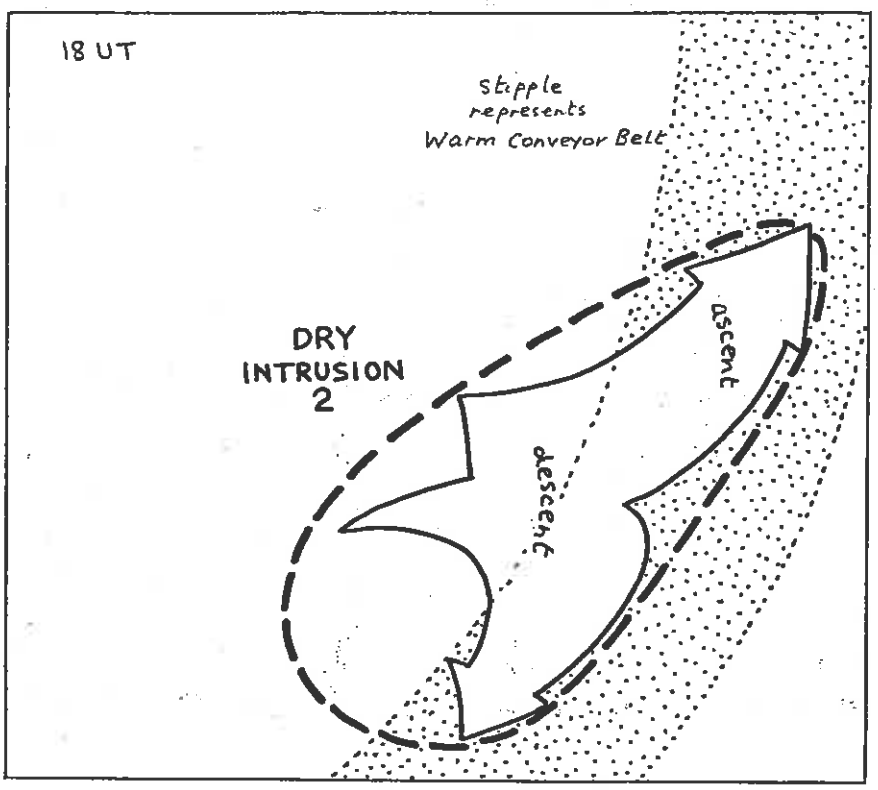


Fig 10(c)

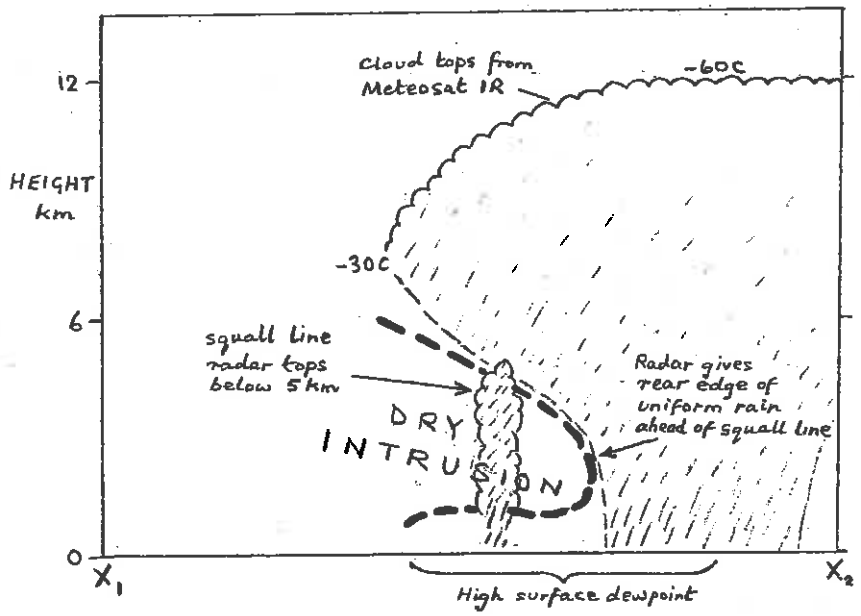
12
HEIGHT
km
6
0
X1
X2
Cloud tops from
Meteosat IR
-60C
-30C
squall line
radar tops
below 5 km
DRY
INTRUSION
Radar gives
rear edge of
uniform rain
ahead of squall line
High surface dewpoint

Fig 10(b)

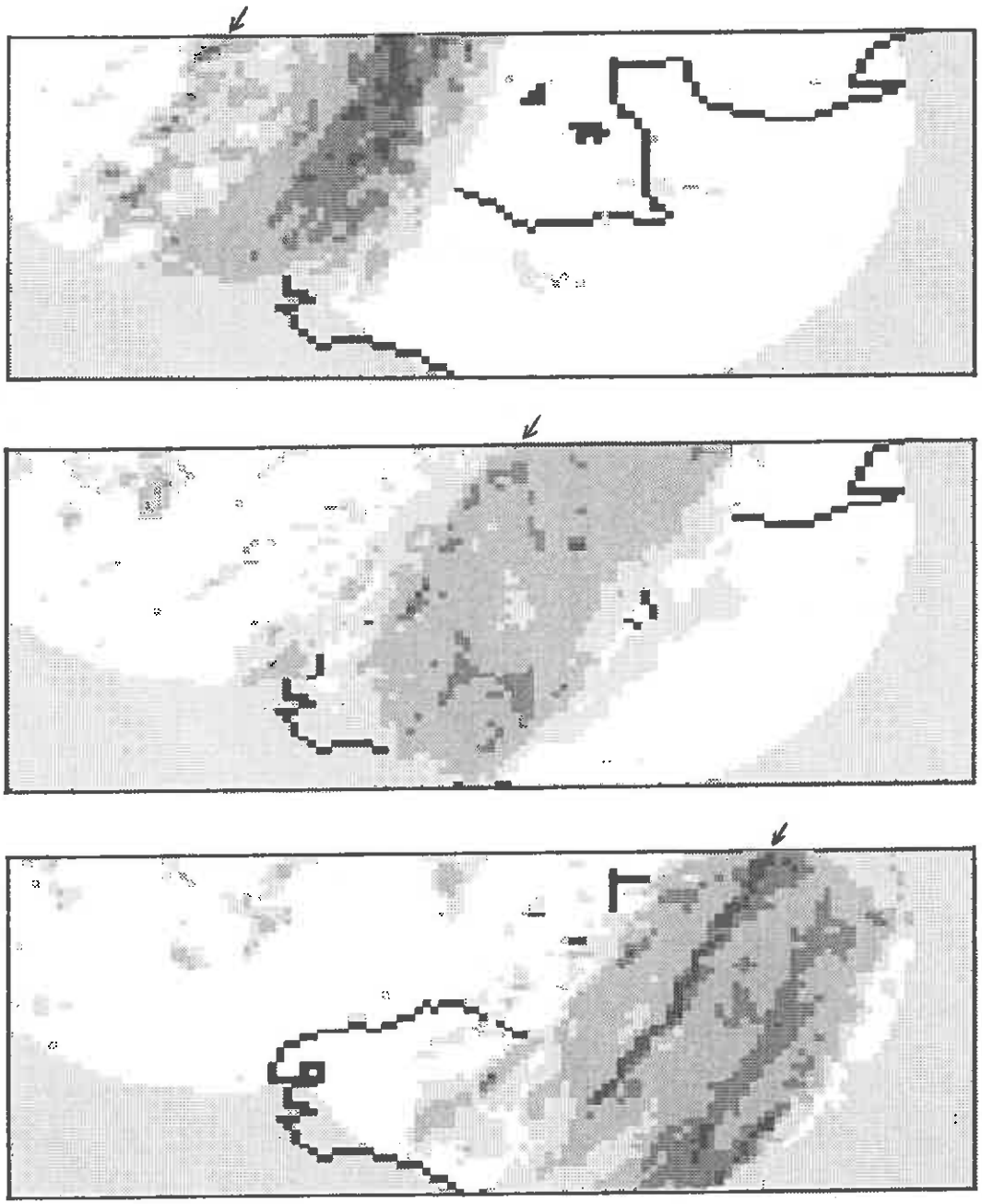

Fig 11

Fig 12

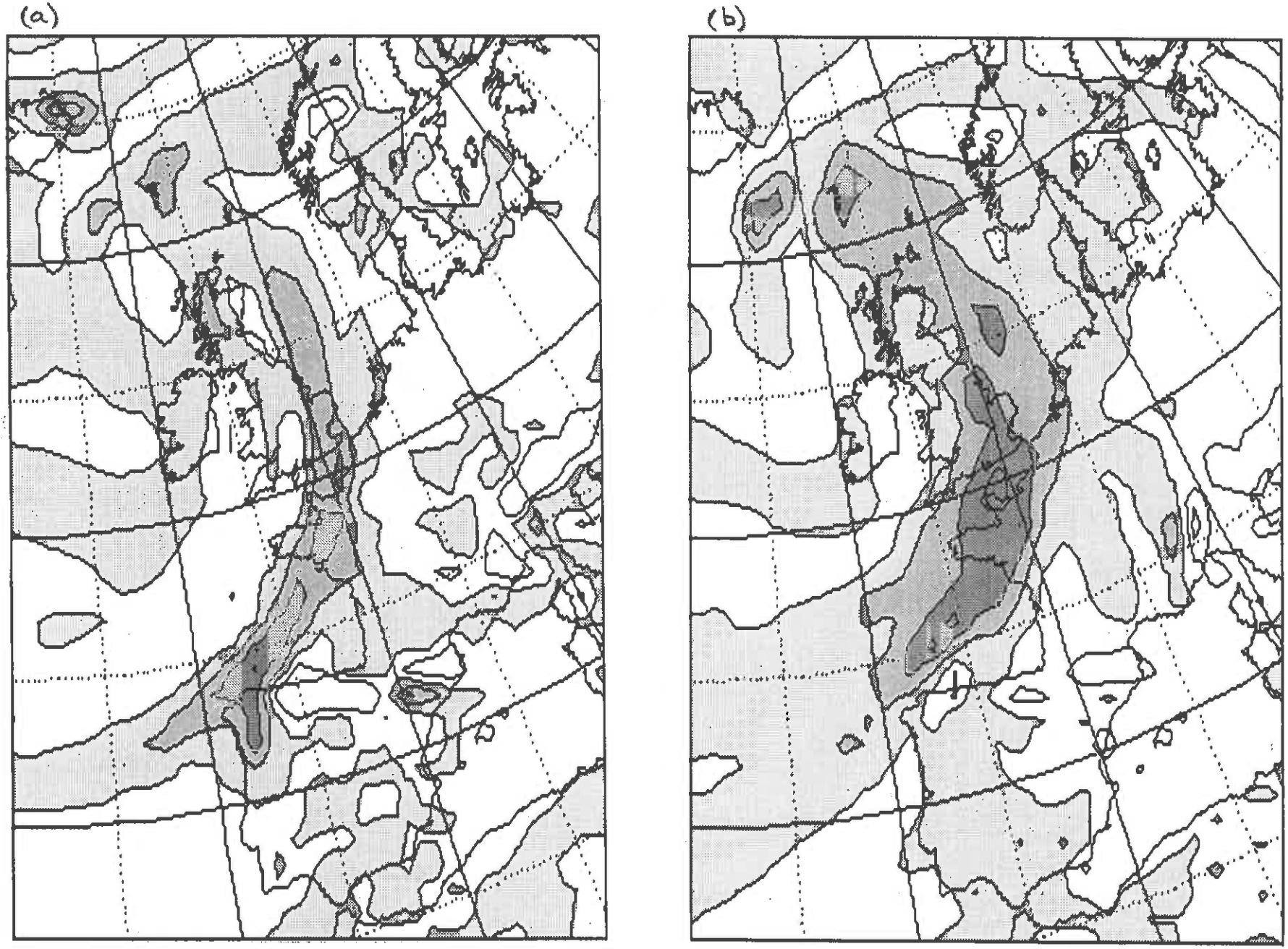

Fig 13

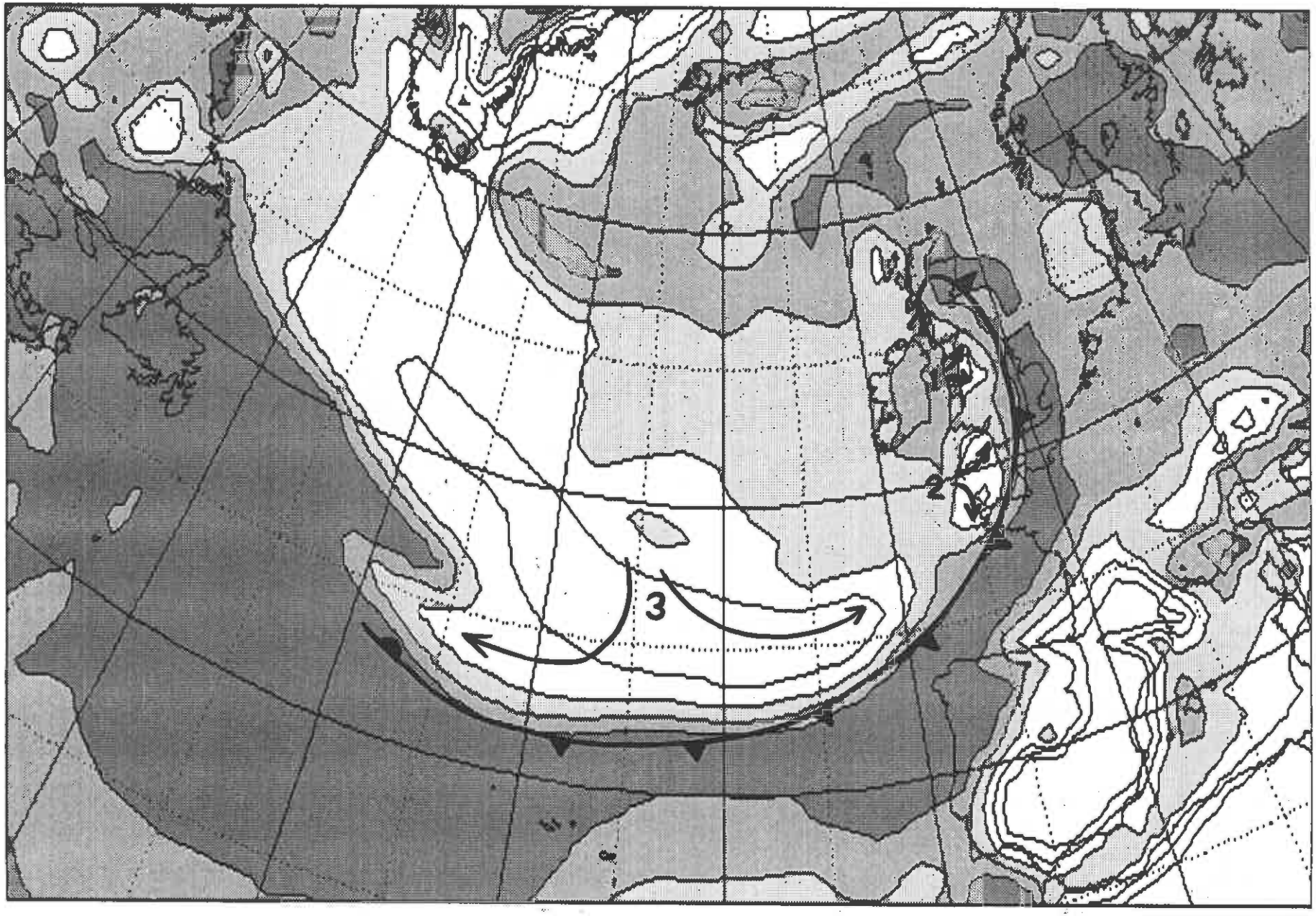

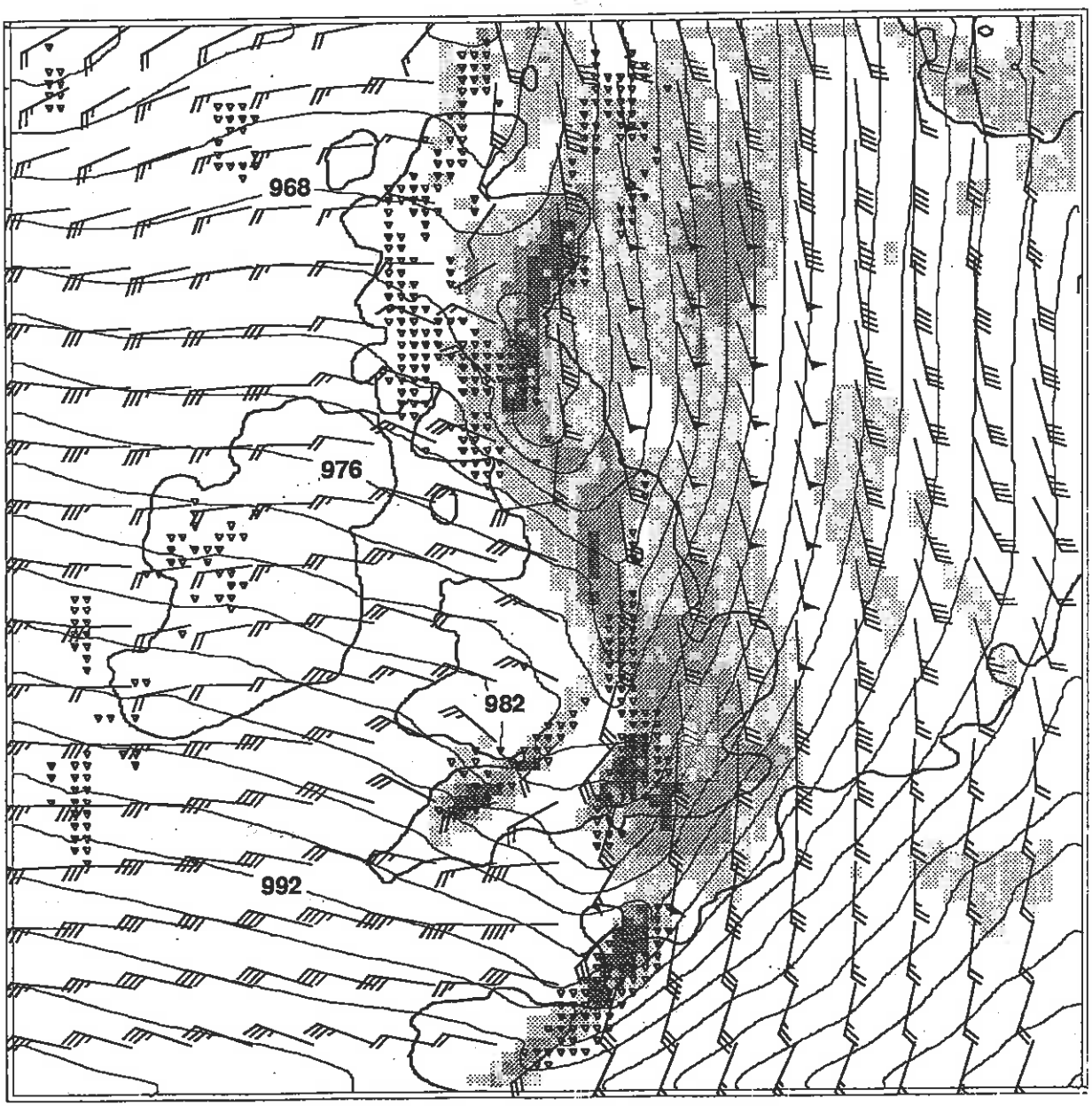


Fig 14

Fig 15(a)

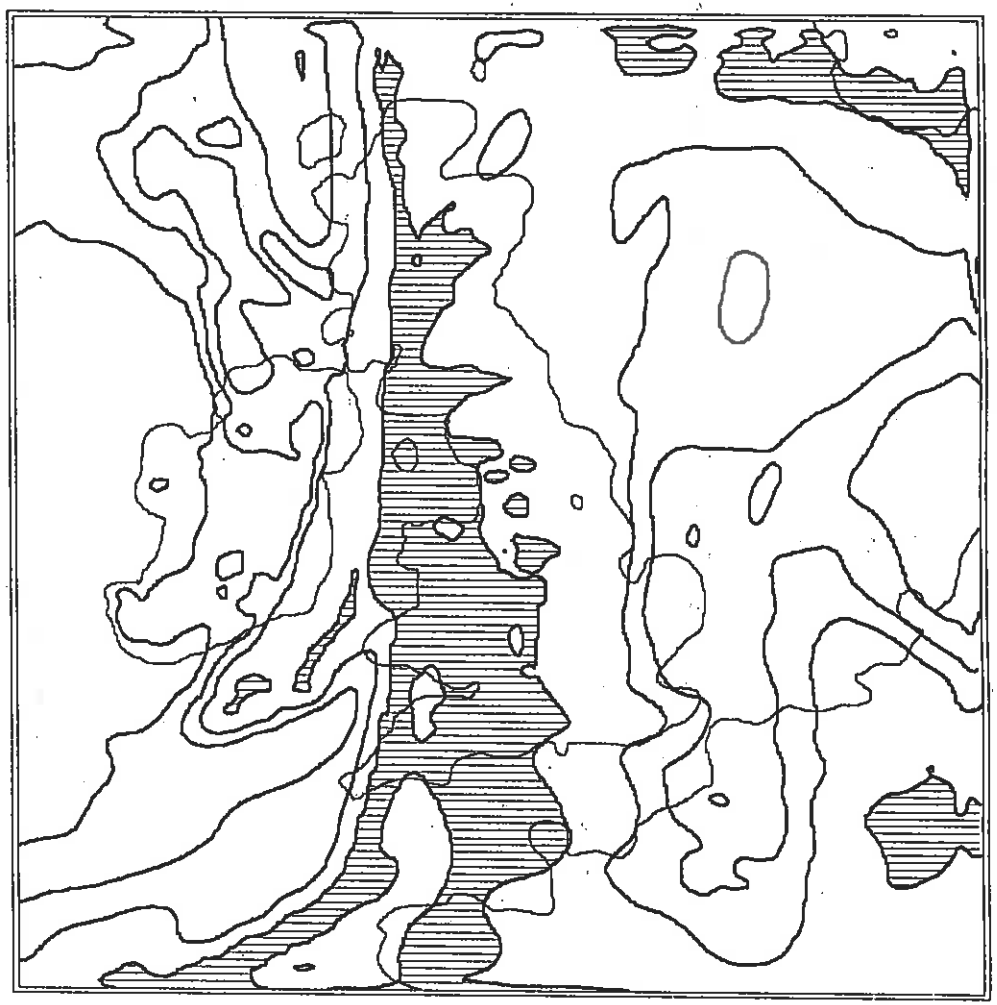

Fig 15(b)

Fig 15(c)

Fig 15(d)

Fig 16

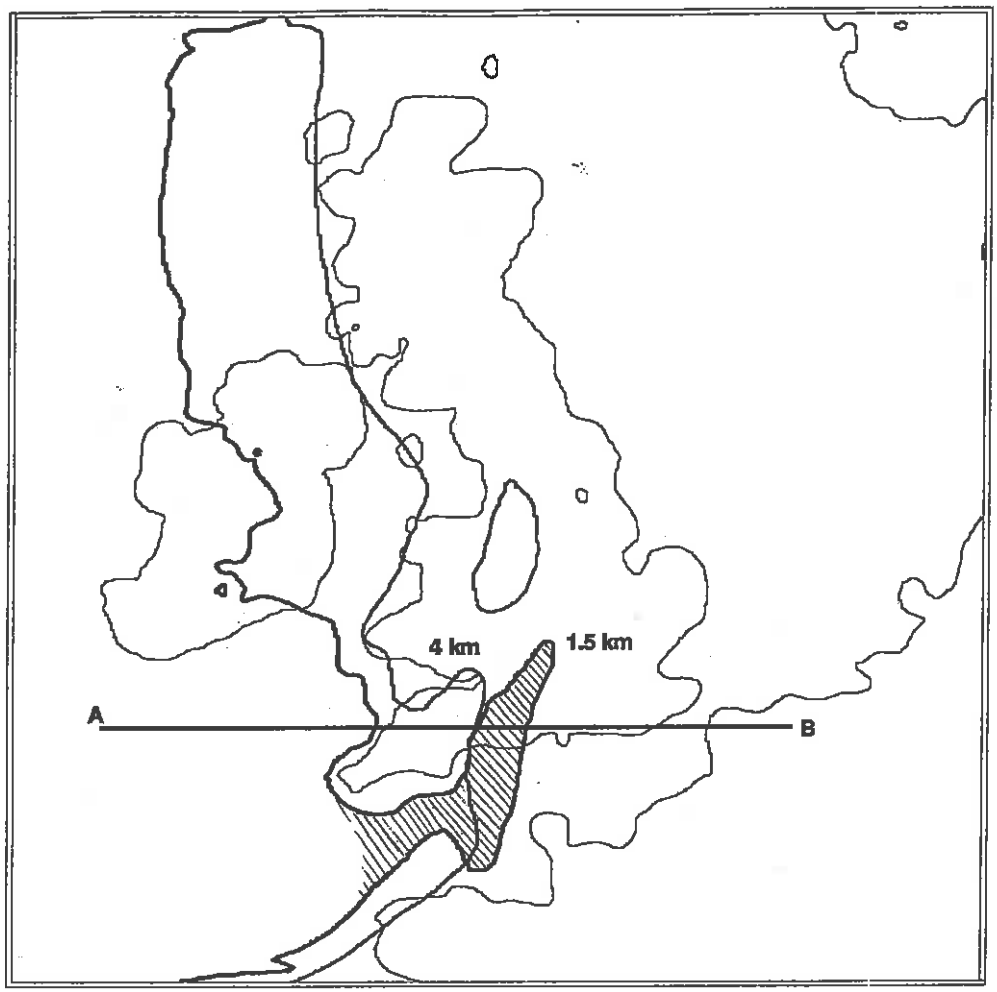


Fig. 17

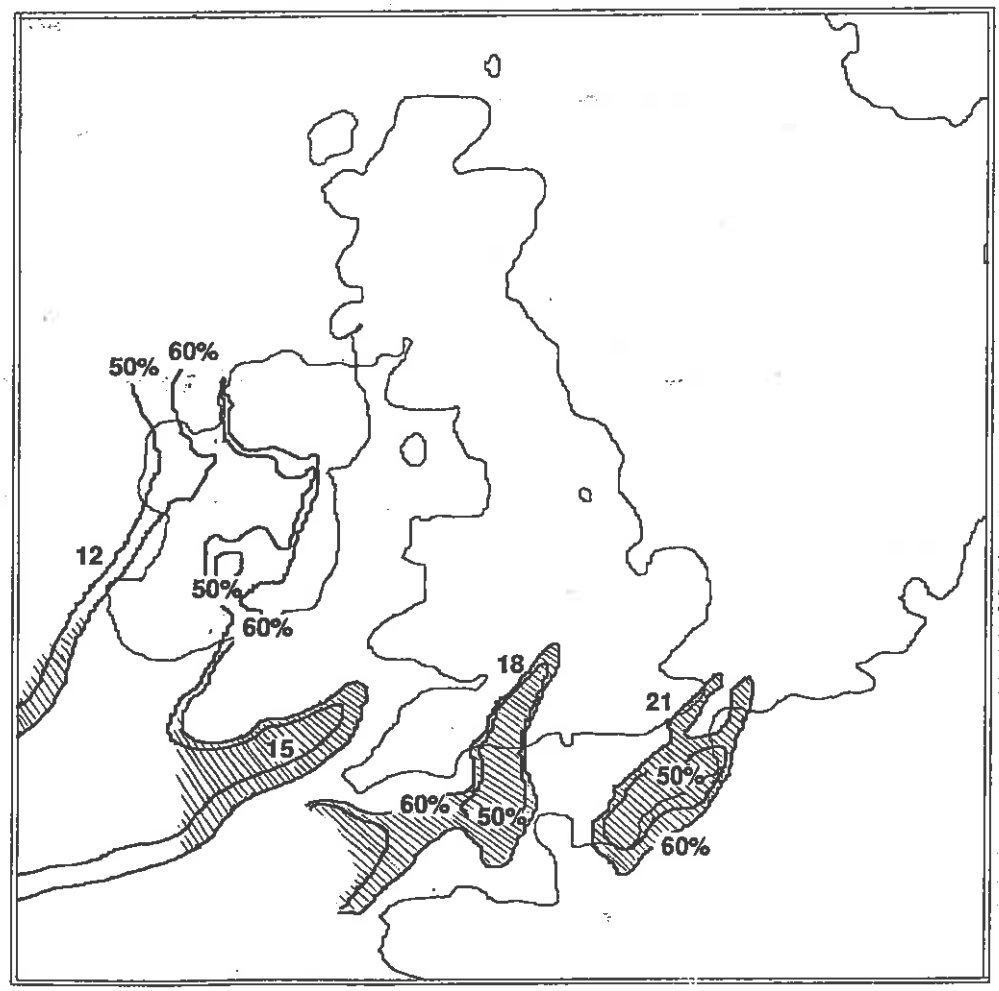

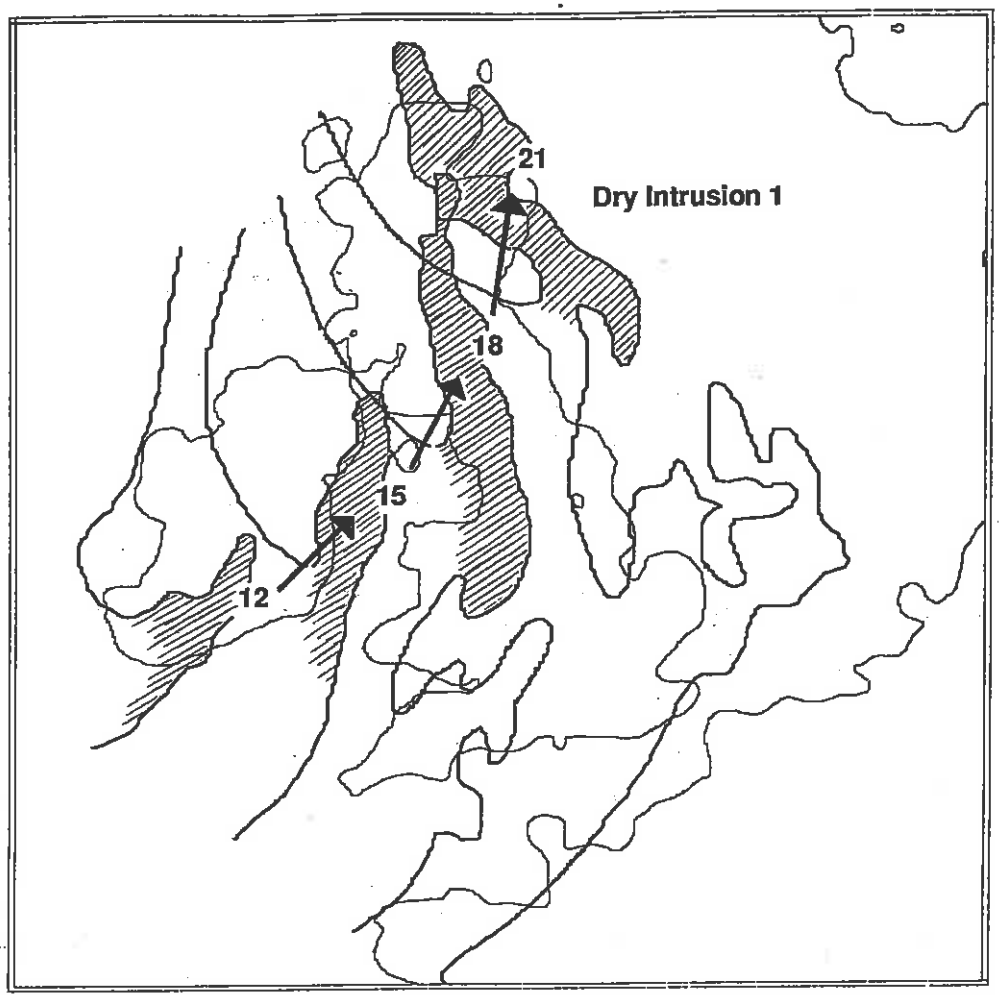


Fig 18(a)

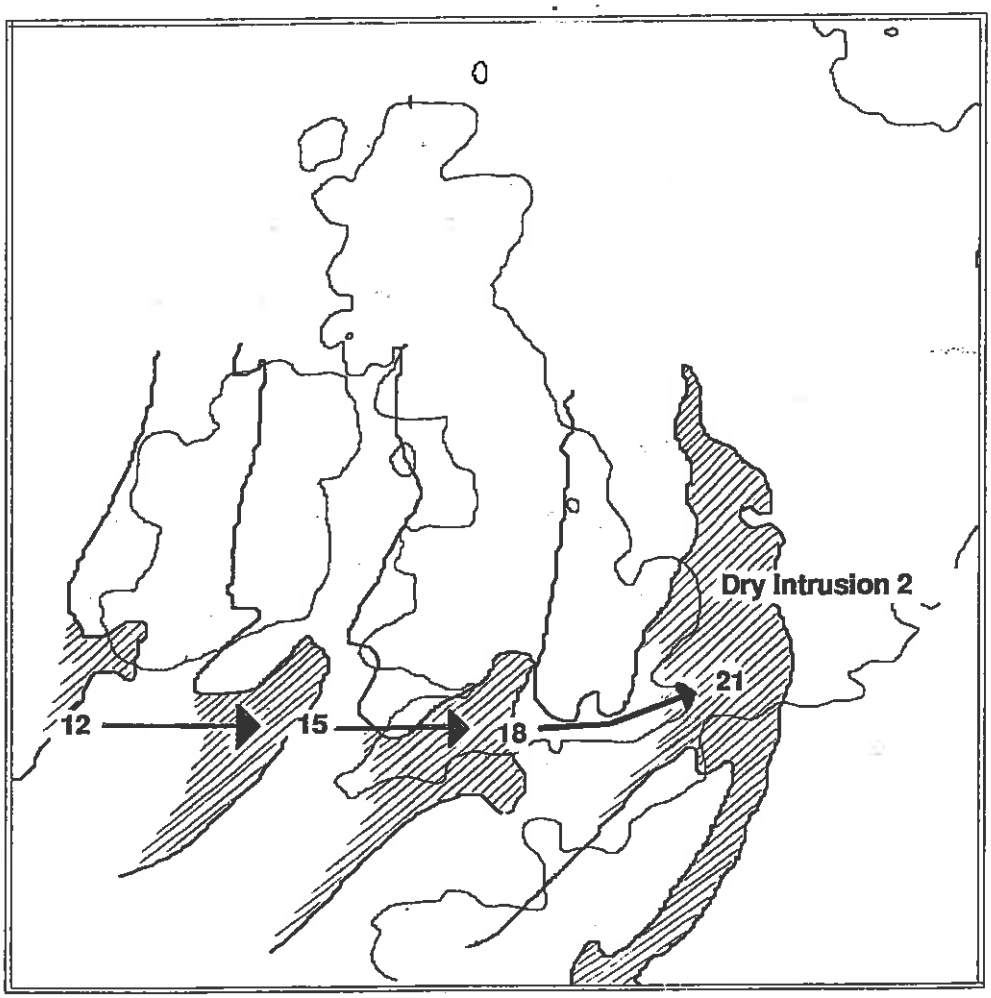


Fig 18(b)

Fig 19(a)

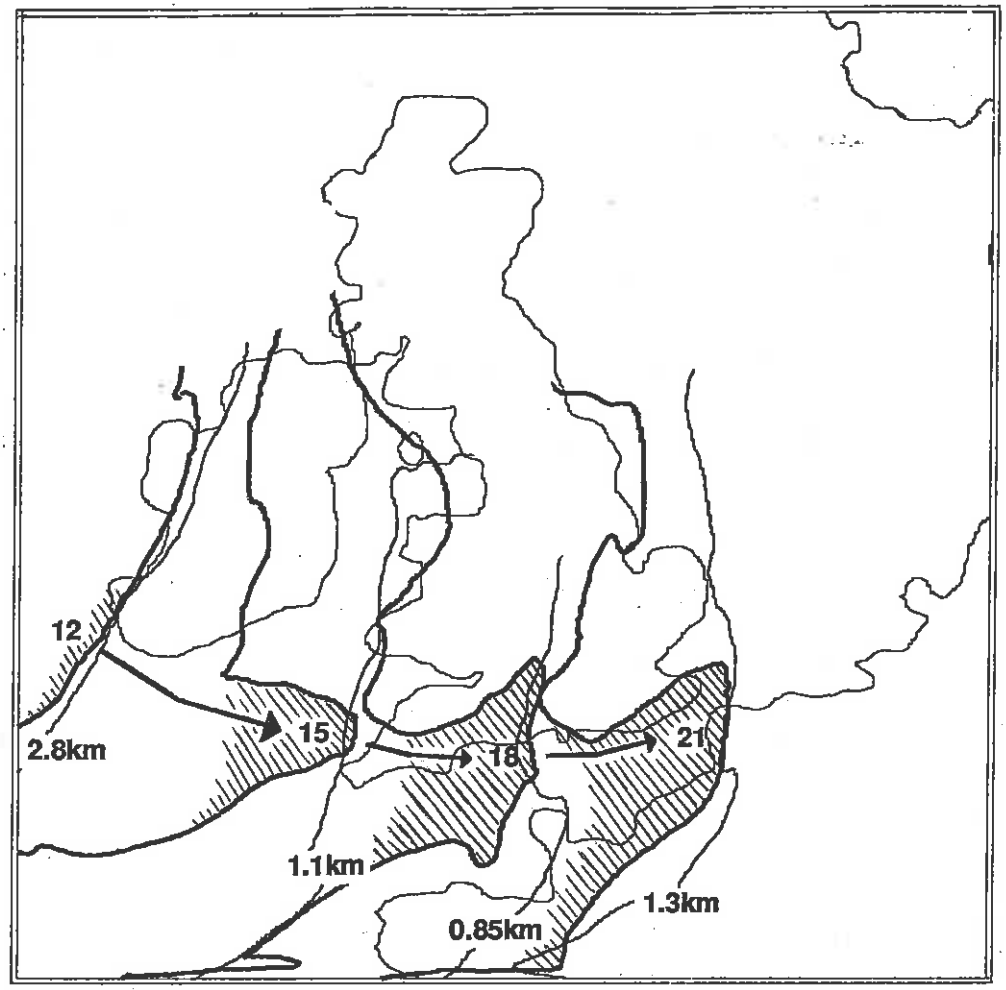


Fig 19(b)

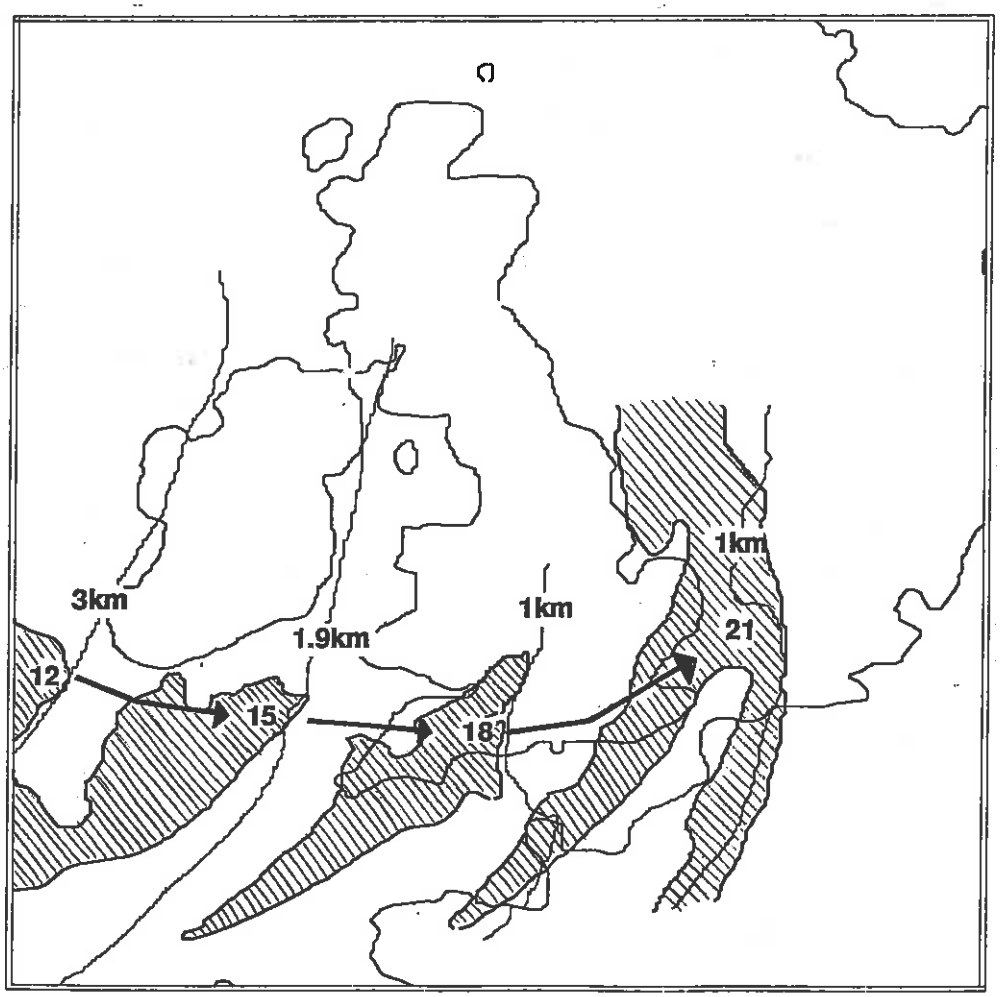

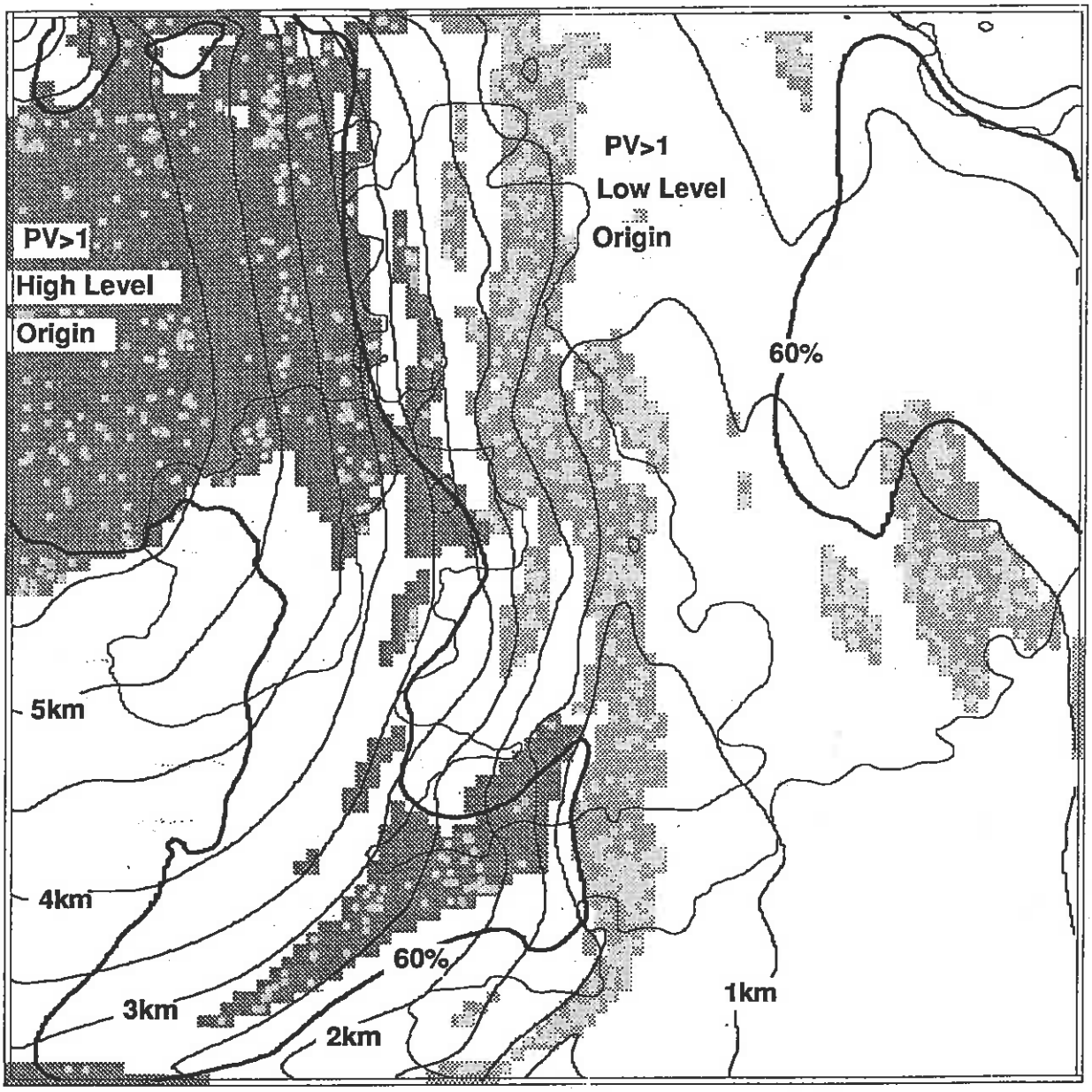
PV>1
High Level
Origin
PV>1
Low Level
Origin
60%
5km
4km
60%
3km
2km
1km

Fig 20

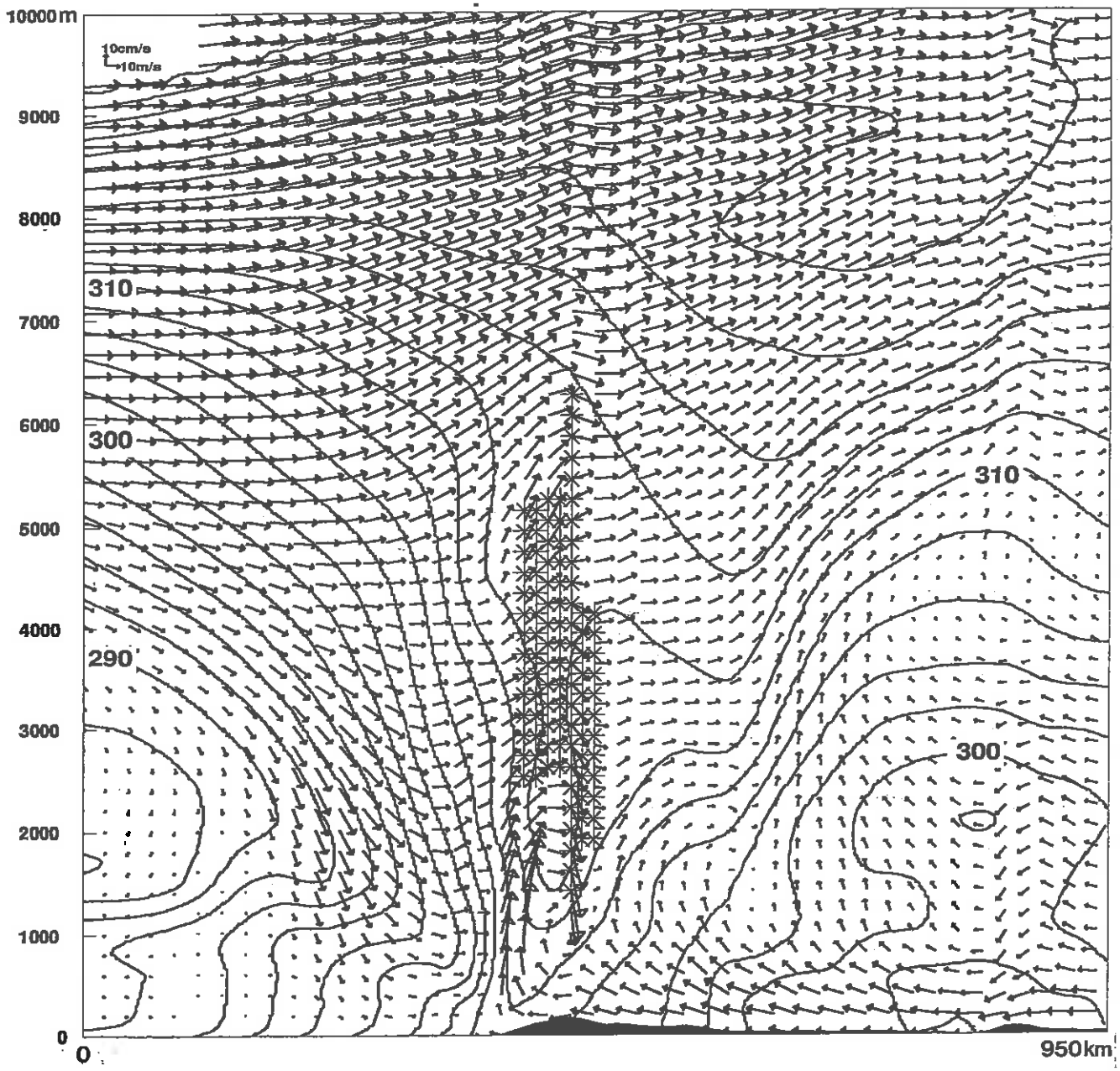
10000m
9000
8000
7000
6000
5000
4000
3000
2000
1000
0
0
950km
10cm/s
10m/s
310
300
290
310
300

Fig 21(a)

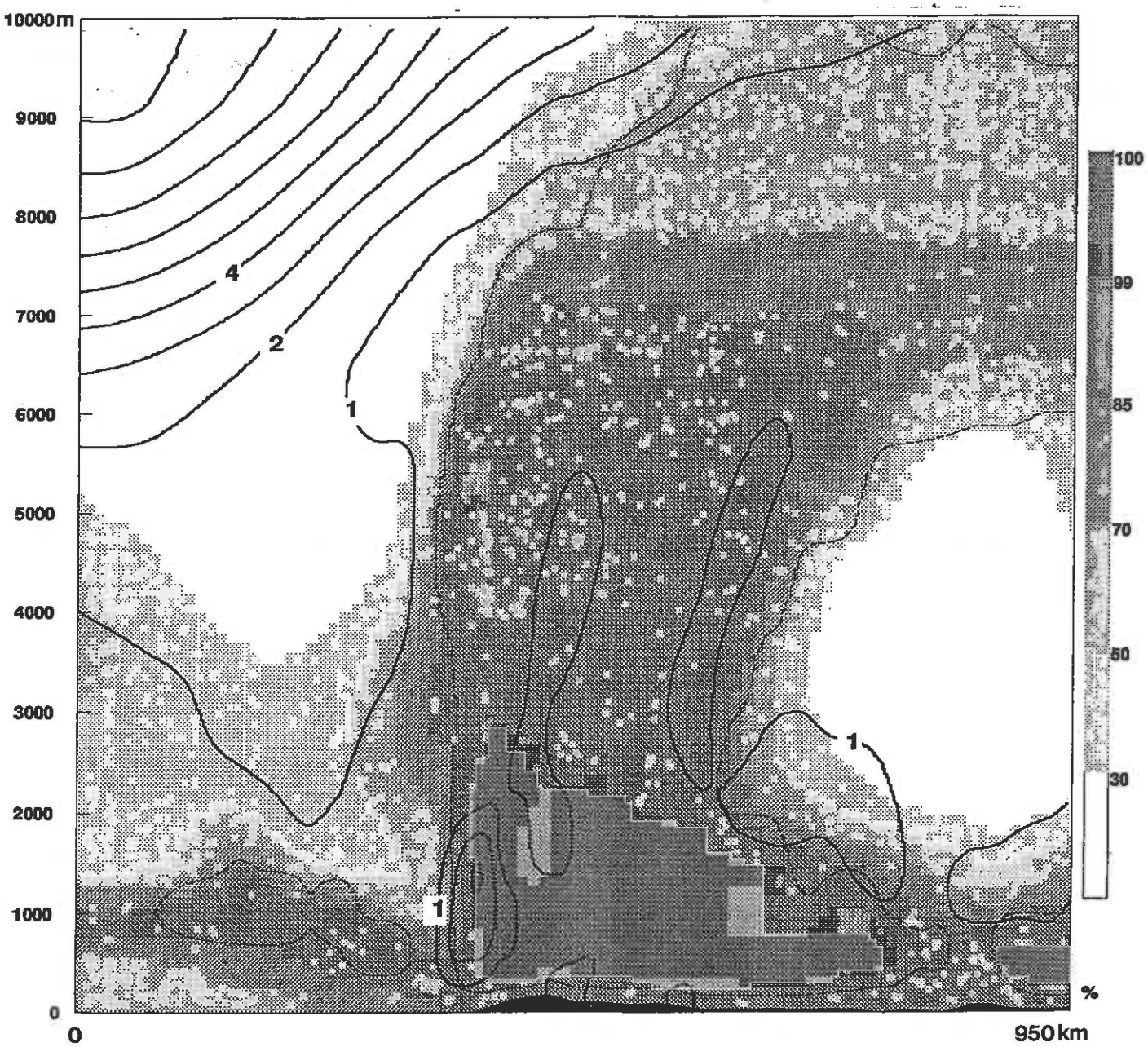
10000m
9000
8000
7000
6000
5000
4000
3000
2000
1000
0
0
950km
4
2
1
1
1
100
99
85
70
50
30
%

Fig 21(b)

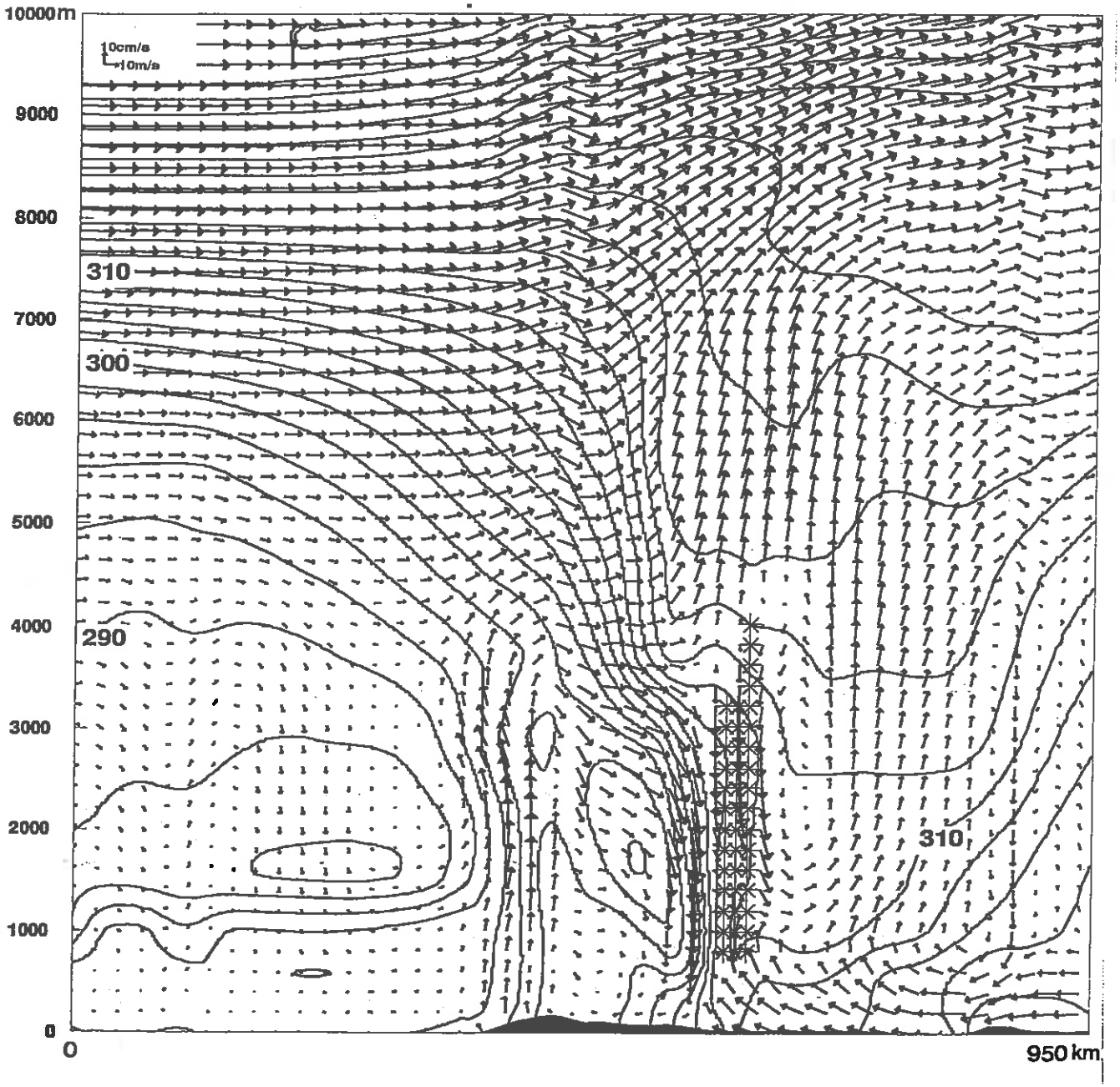
10000m
10cm/s
10m/s
9000
8000
310
7000
300
6000
5000
4000
290
3000
2000
310
1000
0
0
950 km

Fig 21(c)

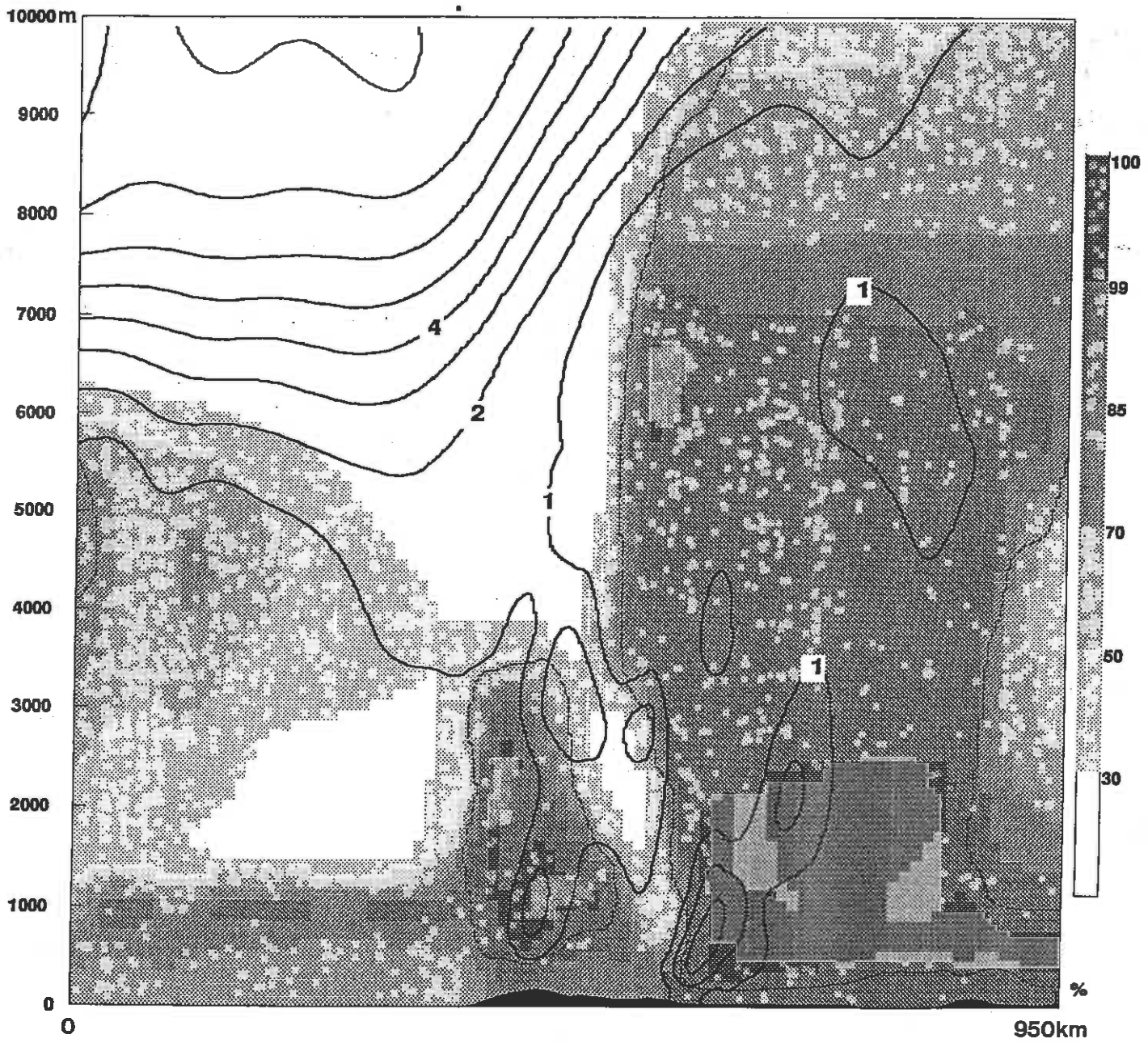
10000 m
9000
8000
7000
6000
5000
4000
3000
2000
1000
0
0
950km
%
100
99
85
70
50
30
1
1
1
2
4

Fig 21(d)

## CURRENT JCMM INTERNAL REPORTS

This series of JCMM Internal Reports, initiated in 1993, contains unpublished reports and also versions of articles submitted for publication. The complete set of Internal Reports is available from the National Meteorology Library on loan, if required.

1. **Research Strategy and Programme.**
   K A Browning et al
   January 1993

2. **The GEWEX Cloud System Study (GCSS).**
   GEWEX Cloud System Science Team
   January 1993

3. **Evolution of a mesoscale upper tropospheric vorticity maximum and comma cloud from a cloud-free two-dimensional potential vorticity anomaly.**
   K A Browning
   January 1993

4. **The Global Energy and Water Cycle**
   K A Browning
   July 1993

5. **Structure of a midlatitude cyclone before occlusion.**
   K A Browning and N Roberts
   July 1993

6. **Developments in Systems and Tools for Weather Forecasting.**
   K A Browning and G Szejwach
   July 1993

7. **Diagnostic study of a narrow cold frontal rainband and severe winds associated with a stratospheric intrusion.**
   K A Browning and R Reynolds
   August 1993

8. **Survey of perceived priority issues in the parametrizations of cloud-related processes in GCMs.**
   K A Browning
   September 1993

9. **The Effect of Rain on Longwave Radiation.**
   I Dharssi
   September 1993

10. **Cloud Microphysical Processes - A Description of the Parametrization used in the Large Eddy Model.**
    H Swann
    October 1993

11. **An Appreciation of the Meteorological Research of Ernst Kleinschmidt.**
A J Thorpe
May 1992

12. **Potential Vorticity of Flow Along the Alps.**
A J Thorpe, H Volkert and Dietrich Heimann
August 1992

13. **The Representation of Fronts.**
A J Thorpe
January 1993

14. **A Parametrization Scheme for Symmetric Instability: Tests for an Idealised Flow.**
C S Chan and A J Thorpe
February 1993

15. **The Fronts 92 Experiment: a Quicklook Atlas.**
Edited by T D Hewson
November 1993

16. **Frontal wave stability during moist deformation frontogenesis. Part 1. Linear wave dynamics**
C H Bishop and A J Thorpe
May 1993

17. **Frontal wave stability during moist deformation frontogenesis. Part 2. The suppression of non-linear wave development.**
C H Bishop and A J Thorpe
May 1993

18. **Gravity waves in sheared ducts.**
S Monserrat and A J Thorpe
October 1993

19. **Potential Vorticity and the Electrostatics Analogy: Quasi-Geostrophic Theory.**
C Bishop and A J Thorpe
November 1993

20. **Recent Advances in the Measurement of Precipitation by Radar.**
A J Illingworth
April 1993

21. **Micro-Physique et Givrage. Cloud Microphysics and Aircraft Icing.**
A J Illingworth
May 1993

22. **Differential Phase Measurements of Precipitation.**
M Blackman and A J Illingworth
May 1993

23. **Estimation of Effective Radius of Cloud Particles from the Radar Reflectivity.**
N I Fox and A J Illingworth
May 1993

24. **A Simple Method of Dopplerising a Pulsed Magnetron Radar.**
L Hua, A J Illingworth and J Eastment
November 1993

25. **Radiation and Polar Lows.**
George C Craig
February 1994

26. **Collected preprints submitted to International Symposium on the Life Cycles of Extratropical Cyclones; Bergen, Norway, 27 June - 1 July 1994**
April 1994

27. **Convective Frontogenesis**
Douglas J Parker, Alan J Thorpe
April 1994

28. **Improved Measurement Of The Ice Water Content In Cirrus Using A Total Water Evaporator**
Philip R A Brown, Peter N Francis
April 1994

29. **Mesoscale Effects of a Dry Intrusion within a Vigorous Cyclone**
K A Browning, B W Golding
April 1994

**Met Office** Joint Centre for Mesoscale Meteorology Department of Meteorology
University of Reading PO Box 243 Reading RG6 6BB United Kingdom
Tel: +44 (0)118 931 8425 Fax: +44 (0)118 931 8791
www.metoffice.com